

24. LITHOLOGY, PETROGRAPHY, AND MINERALOGY OF BASALTS FROM DSDP SITES 482, 483, 484, AND 485 AT THE MOUTH OF THE GULF OF CALIFORNIA¹

Brendon J. Griffin, Electron Optical Center, University of Adelaide, Box 498, G.P.O. Adelaide, South Australia 5001 and

Rolf D. Neuser and Hans-Ulrich Schmincke, Institut für Mineralogie, Ruhr-Universität, 4630 Bochum, Federal Republic of Germany

ABSTRACT

The majority of the basalts drilled on Leg 65 in the Gulf of California are aphyric to sparsely phyrlic massive flows ranging in average thickness between 5 meters in the upper part of the sections in Holes 483 and 483B, where they are interlayered with sediment, and 14 meters in Hole 485A, where interlayered sediments constitute more than half of the section. Massive flows interlayered with pillows are generally less than 4 meters thick. The pillow lavas recovered are more phyrlic (up to 15 modal%) and contain two to three generations of plagioclase and olivine ± clinopyroxene. Plagioclase generally exceeds 60% of any given phenocryst assemblage. Resorbed olivine, clinopyroxene, and plagioclase megacrysts may reflect a high-pressure stage, the phenocrysts crystallizing in the main magma chamber and the skeletal microphenocrysts in dikes. Precise measurements of length/width ratios of different phenocryst types and compositions show low aspect ratios and large crystal volumes for early crystals and high ratios and low volumes for late crystals grown under strong undercooling conditions. The minerals examined show wide ranges in composition: in particular, plagioclase ranges from An₉₂ to An₃₆; clinopyroxene ranges from Ca₄₁Mg₅₁Fe₈ in the cores of phenocrysts to Ca₄₀Mg₄₃Fe₁₅²⁰ in the groundmass; and olivine ranges from Fo₈₆ to Fo₈₁.

The wide range in mineral compositions, together with evidence of disequilibrium based on textures and comparisons of glass and mineral compositions, indicate complex crystallization histories involving both polybaric crystal fractionation and magma mixing.

INTRODUCTION

During Leg 65 of the Deep Sea Drilling Project (DSDP), six major holes were drilled at three principal sites (482, 483, and 485) at the mouth of the Gulf of California (23°N) (Figs. 1 and 2), recovering a total of about 420 meters of basalt (Figs. 3 and 4). The holes were drilled in crust ranging in age from 0.5 m.y. (Site 482) to 2.0 m.y. (Site 483) at distances ranging from 12 km (Site 482) to 52 km (Site 483) from the spreading axis. One additional site (Site 484) was drilled in the nearby Tamayo Fracture Zone (Fig. 1). One of the main purposes of this leg was to study magma chamber evolution and crustal construction processes at a ridge with a moderately high spreading rate (about 5 cm/y.) in a young ocean basin with a high sediment influx for comparison with slow spreading ridges (2–3 cm/y.) of the Atlantic type with very low sedimentation rates. The present chapter presents and briefly evaluates lithologic, petrographic, and mineral composition data for basalts from these sites. Major and trace element data are discussed in a companion paper (Flower et al., this volume) and volcanoclastic rocks and glass alteration are discussed by Schmincke (this volume). A fuller discussion of the data will be presented elsewhere.

GENERAL LITHOLOGY

Two principal types of basalt were recovered in the Leg 65 drill sites: massive basalt (Plate 1, Figs. 1–4; Plate 2,

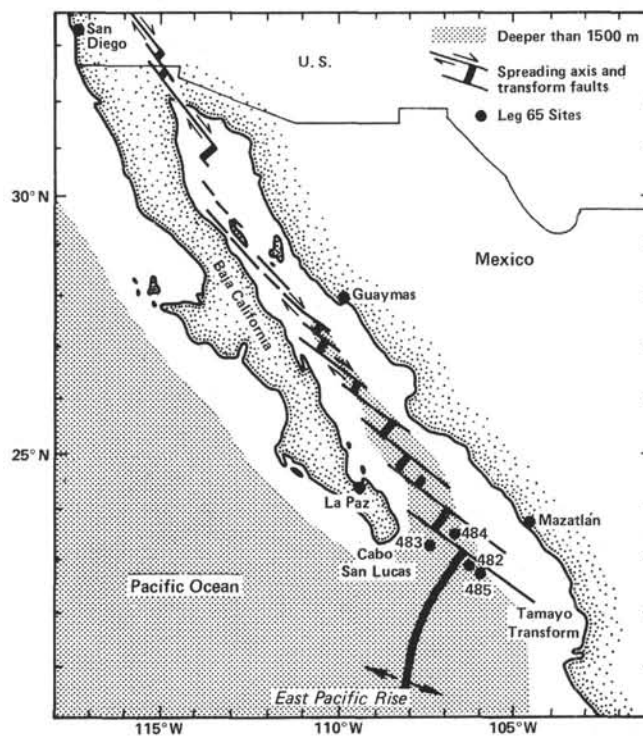


Figure 1. Index map of the Gulf of California showing the main sites drilled during Leg 65.

Figs. 1–3) and pillow basalt (Plate 2, Fig. 4; Fig. 5; Table 1). Most, if not all, of the massive basalts are believed to have been emplaced as sheet flows rather than as sills. This interpretation is based on several lines of evidence,

¹ Lewis, B. T. R., Robinson, P., et al., *Init. Repts. DSDP, 65*: Washington (U.S. Govt. Printing Office).

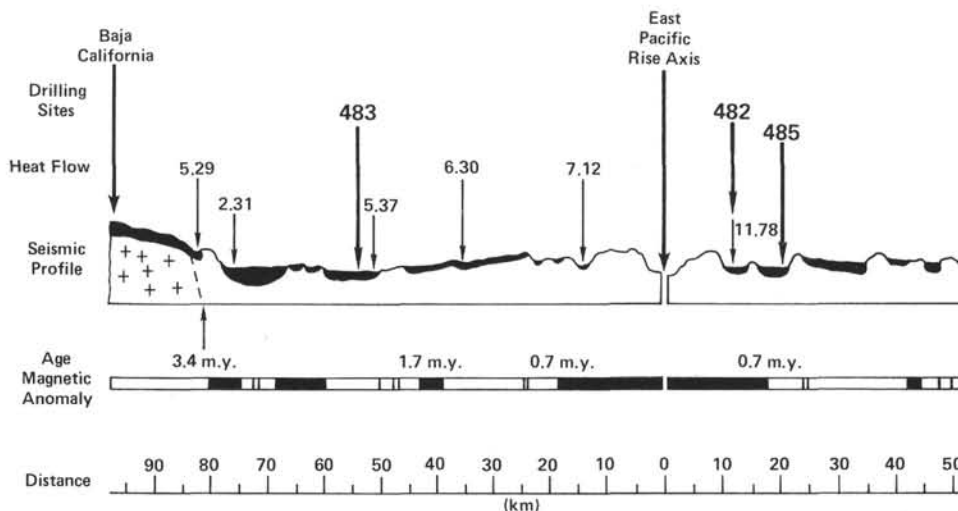


Figure 2. Cross section from Baja California through the East Pacific Rise showing main drill sites, sediment basins (black), heat-flow values, and magnetic anomalies. (Simplified from Lewis, this volume.)

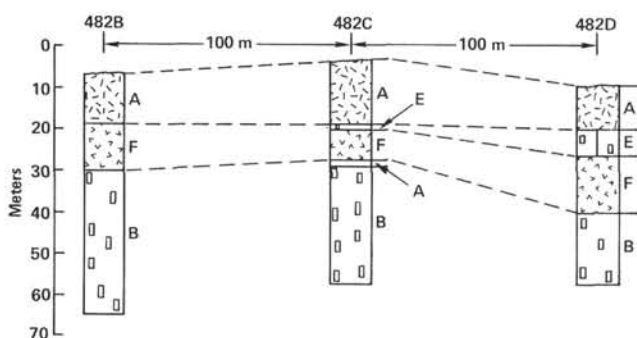


Figure 3. Stratigraphic correlation of main lithologic and chemical units between three holes drilled at Site 482. (A, B, E, and F represent chemical (or magma) types defined by Flower et al., this volume.)

including the following: (1) the presence of a distinctly vesicular zone below the top of the massive basalts (Plate 2, Figs. 1–3); (2) the absence of intrusive relationships; (3) the absence of baked contacts (the minor induration observed in the sediments immediately overlying several of the massive basalt units is attributed to subsequent diagenetic reactions near the sediment/basalt contact) (Plate 1, Figs. 1, 2); (4) the presence in one hole of a bedded hyaloclastite which chemically resembles the underlying massive basalt, suggesting derivation from the glassy crust of a surface flow (Schmincke, this volume); (5) the stratigraphic continuity over distances of several hundred meters of flows which are vertically separated from other massive units by a few centimeters to a few meters of sediment (Fig. 3); (6) the imprint of broken vesicles in the sediments lying in contact with the underlying basalt; and finally (7) the presence of ophi-mottled textures in the basalts themselves (Robinson et al., 1980).

Other lines of evidence, however, such as internal diking in Unit 3, Hole 483 (Plate 1, Fig. 4) and chemical differences within Unit 5, Hole 485 (Flower et al., this volume) suggest intrusive processes. In lithologic Unit 3

(Hole 483) the diking could have occurred as autointrusion during the sagging of a thick, liquid-cored lava sheet after it was emplaced on soft sediment. The chemical diversity within Lithologic Unit 5 (Hole 485A), however, is probably the result of the intrusion of magma batches of slightly differing chemistry. Thin stringers of sideromelane extending into the sediment from the top of Lithologic Unit 8 in Hole 485A also suggest intrusion (Plate 1, Fig. 3). The sites drilled are thus intermediate between an environment with a high sedimentation rate, such as the Guaymas Basin, in which many if not all of the basalts are emplaced as intrusives (Curry, Moore, et al., in press) and one with a low sedimentation rate, such as the Mid-Atlantic Ridge, where nonintrusive sheet flows are common (e.g., Robinson et al., 1980). A further indirect but powerful argument for the interpretation of the massive basalts as extrusives is the succession of flows observed in Holes 483 and 483B in which massive flows of more evolved chemistry and mineralogy are underlain by pillow lavas of more mafic chemistry and higher phenocryst content (Flower et al., this volume). The massive basalt flows are from 3 to 7 meters thick in the upper part of Holes 483 and 483B above the pillows, but are much thicker in Hole 485A where the average thickness is about 10 to 14 meters (excluding Unit 5, which is 26 m thick). We are not certain whether thick sheet flows and intrusives grade into each other where surface flows have burrowed into soft sediments. In any case, thick massive flows appear to dominate during the late and probably waning stage of volcanism. They represent single extrusive events separated from each other by a significant hiatus in time. The sheet flows interbedded with pillow lavas in the lower part of Holes 483 and 483B (Fig. 4) are thinner and more vesicular than the flows higher in the section and are separated from each other and the overlying pillows by much thinner sediment layers. The pillow sequences are also thin (about 15 m). Although sheet flow and pillow units could represent the distal edges of eruptive units, the similarity in the thickness of the units between Holes

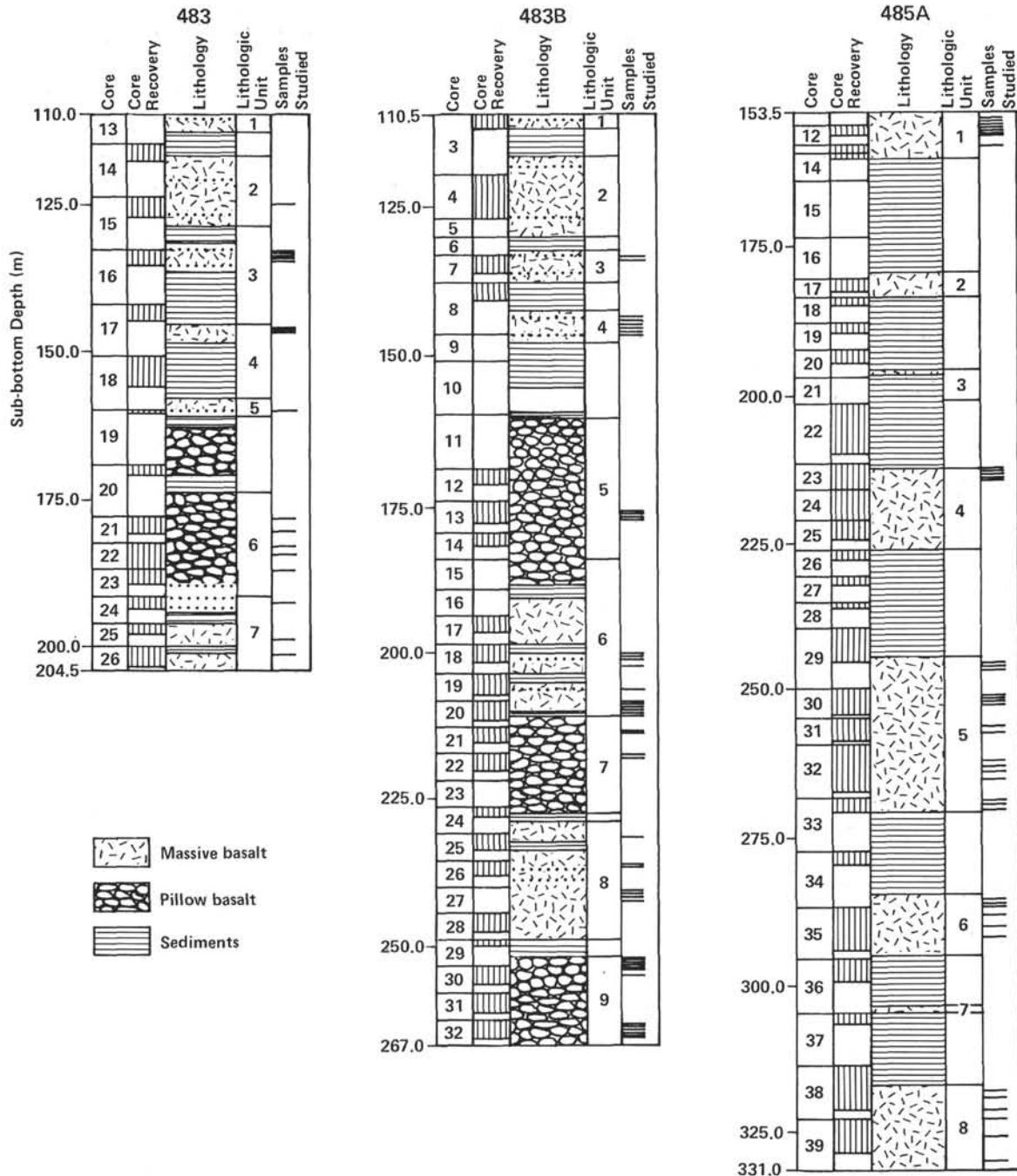


Figure 4. Stratigraphic columns for Holes 483, 483B, and 485A showing core recovery, main igneous lithologic units, and position of samples studied. Extent of igneous units defined by logs (Hole 483) and drilling rates (Hole 485A) is greater than recovered portion.

Table 1. Comparison of characteristic features of massive and pillow basalt flows drilled on Leg 65.

Basalt	Thickness (m)	Phenocrysts (vol.%)	Contacts	Thickness of Glassy Rinds (cm)	Fractures
Massive (sheet) flows	1.0-10.0	2	Flat	0.5	Straight
Pillow (tube) flows	0.4-0.5	5-15	Curved	1-2	Irregular

483 and 483B, about 100 meters apart (Fig. 4), as well as between Holes 482B, C, and D where the holes are about 200 meters apart (Fig. 3), suggests that the eruptive units are relatively thin in this environment. In other words, the height of sheet flow and pillow volcanoes during terminal activity at the mouth of the Gulf of California appears to have been low.

One of the factors determining volcano height appears to be spreading rate; volcano heights range from

about 250 meters in the FAMOUS area to 50 meters in the Galapagos Rift (Ballard et al., 1979). Eruptive units, as well as eruptive cycles combining several petrologically related eruptive units, appear to be thicker in the Atlantic than in the Pacific, judging from the deepest holes drilled on Legs 37 and 51–53 (Flower and Robinson, 1979, 1981; Robinson et al., 1980).

Robinson et al. (1980) restrict the term "flow" to cooling units more than 3 meters thick. While such thicknesses hold for flows in the upper part of Holes 482, 483, 483B, and all of Hole 485A, several massive basalt units interlayered with pillows in the lower part of Holes 483 and 483B have been interpreted as flows even though they are less than three meters thick. We have observed flows of similar thickness to be common in the Troodos extrusive section (Schmincke et al., in press).

The reason why submarine lavas erupt as pillow and sheet flows is not clear, but high eruptive rates are thought to be an important factor (Ballard, 1979; Robinson et al., 1980). The lateral continuity of individual flows over at least 200 meters at two sites (482 and 483) also suggests that these flows represent high eruptive rates.

PETROGRAPHY

METHODS

About 60 thin sections, representing all holes and all major basalt types, were first examined qualitatively using a petrographic microscope. Twenty thin sections, chiefly of glassy to tachylitic basalts, were then studied quantitatively using the semi-automatic VIDEOPLAN picture-analysis system, which allows precise measurement of the volume, size, and form of phenocryst phases. Two methods of measuring crystal dimensions were employed in this study. In the first method, thin sections were projected onto a digitizing tablet and the phenocryst perimeters were then traced with an electronic pen. In the second method, the light from a light-emitting diode (LED) attached to an electronic cursor is projected into the measuring field of the microscope. Thus the movements of the cursor on the digitizing tablet can be followed while observing the thin section. The longest and shortest dimensions were then calculated for each crystal from the major (A) and minor (B) axes of the ellipse with the same moment of inertia as that of the measured grain. In each thin section, up to six areas about 0.8 cm in diameter were measured, covering from 50% to 80% of the area.

Pillow basalts were selected for more detailed examination in this study because they tend to be more phyric than massive basalts and because phenocrysts can be more easily identified in rocks with a glassy or fine-grained groundmass. The data from this analysis are reported in Table 2 and in Figures 5 through 9.

General Petrographic Overview

The basalts drilled on Leg 65 show the entire range of submarine basalt textures, from thick, fresh, glassy pillow rinds (Plate 2, Fig. 4) and thin, mostly devitrified margins of massive flows (Plate 1, Figs. 1, 2) to coarse-grained gabbros in the 10- to 20-meter-thick cooling units recovered at Site 485. Most of the basalts are aphyric to sparsely phyric, but phyric basalts with 5% to 15% total phenocrysts are common in the pillowed units of Holes 483 and 483B (Table 2) and in the lowermost massive flows in Hole 483. Like most ocean floor basalts, the most common phenocryst phase is plagioclase, which generally composes from 60% to 90% of the phenocryst assemblage. Olivine is generally less abundant ($\leq 3\%$ in

volume), and clinopyroxene is usually sparse ($\leq 1\%$) to absent. Clinopyroxene is more common than olivine, however, in Cores 483B-22 through 25, where it occurs principally in glomerophyric intergrowths with plagioclase, indicating more advanced crystallization of the magma prior to eruption.

Vesicles are rare to absent in the chilled margins examined but increase in size and abundance toward the interiors of pillows and the tops of sheet flows, averaging less than 2% by volume. Segregation vesicles, on the other hand, are very common in both types of basalt (Plate 2, Figs. 1–3). These become increasingly filled toward the interiors of pillows and may be rimmed with plagioclase.

Pervasive alteration is generally restricted to the filling of vesicles (Plate 2, Figs. 1–3) and fractures, and to the replacement with smectite of groundmass glass and most of the olivine in the more coarse-grained basalts. Higher-grade alteration occurs near a hydrothermal vein in Hole 482C and in the interior of several thick cooling units at Site 485 (Morrison and Thompson, this volume).

Phenocrysts

Plagioclase

Plagioclase occurs in four texturally and compositionally distinct forms in the Leg 65 basalts. These consist of megacrysts, normal phenocrysts, microphenocrysts, and microlites.

Plagioclase I (megacrysts): (Plate 3, Figs. 1, 2). The plagioclase megacrysts observed occur almost exclusively in the phyric pillow basalts of Holes 483 and 483B where they generally constitute less than 1% of the rock. They are classified as megacrysts not because of their abnormal size (54 mm) but because they are larger than the other plagioclase types, occur mostly as single crystals, are moderately to strongly rounded, may have cores filled with, or delineated by, devitrified melt inclusions, and show complex, in part oscillatory zoning with one or more major breaks in composition. The crystals vary in area from about 5 to 20 mm² with a mean value of 10.5 mm² and have an aspect ratio, A/B, which is always less than 3 (Figs. 6, 7).

Plagioclase II (normal phenocrysts): (Plate 3, Fig. 3). Normal phenocrysts constitute between 6% and 8% of the most phyric basalts and range in length from 0.1 to 0.3 mm, with most averaging 0.7 mm. The phenocrysts vary in area from 0.3 to 10 mm² with a mean of 1.5 mm² and have a maximum aspect ratio of 8 (Figs. 6 and 7). The crystals are invariably euhedral and commonly display synneis twinning. Zoning, however, is not pronounced. The plagioclase in this group may occur in glomerocrysts with olivine but crystals intergrown with clinopyroxene are also included in this group, though they are mostly sub- to anhedral. In some basalts, phenocrysts grade irregularly into microphenocrysts.

Plagioclase III (microphenocrysts or pre-eruption microlites): (Plate 3, Fig. 4; Plate 4, Fig. 1). The plagioclase crystals belonging to Group III are generally euhedral and range up to 1.2 mm in length, with most falling between 0.2 and 0.25 mm in length. The crystals are

Table 2. Textures and phenocryst abundances in Leg 65 basalts.

Sample (interval in cm)	Rock Type	Lithologic Unit	Cooling Unit	Chemical ^a Type	Phenocrysts (vol.%, modal)								Glomerocrysts (vol.% modal)			Vesicles	Counted (C); Estimated (E)	Predominant Texture
					Ol I	Ol II	Cpx I	Cpx II	Pl I	Pl II	Pl III	Total	Ol-Pl	Ol-Pl-Cpx	Pl-Cpx			
Hole 482D																		
11-1, 24-28	PT	3	7	F	—	1.3	—	—	—	0.8	4.8	6.9	d			0.1	C	Vitrophyric-variolitic
Hole 483																		
21-1, 49-55	PT	6	13	F	0.2	1.2	0.6	0.1	0.3	6.5	2.1	11.0	d	m	m	0.3	C	Variolitic with segregation vesicles
21-1, 57-61	PC	6	13	F	0.3	0.9	0.2	0.1	1.0	5.5	2.4	10.4	d	m	m	0.6	C	Tachylitic with segregation vesicles
21-1, 78-82	PB	6	13	F	0.8	0.4	—	0.2	1.5	4.8	2.4	10.1	d	m	m	0.2	C	Vitrophyric-tachylitic
21-3, 6-9	PB	6	17	F	1.0	0.8	—	0.2	1.0	3.0	1.0	7.0	d		m	0.1	E	Vitrophyric-variolitic
21-2, 68-72	PT	6	23	F	1.0	0.5	0.1	—	3.1	5.5	1.7	10.2	m		d	0.4	C	Vitrophyric-tachylitic
22-2, 85-88	PC	6	23	F	0.7	0.2	—	0.2	3.0	3.2	1.8	9.1	m		d	2.3	C	Tachylitic with filled segregation vesicles
22-2, 88-93	PC	6	23	F	0.2	1.2	0.7	0.1	1.5	4.0	2.7	10.4	m		d	0.5	C	Tachylitic with open segregation vesicles
22-2, 94-99	PB	6	23	F	0.5	0.6	1.3	—	1.0	5.0	2.9	11.3	m		d	1.5	C	Tachylitic with filled segregation vesicles
Hole 483B																		
20-2, 37-42	SB	6	26	H	0.3	0.5	—	—	—	1.5	—	2.3				0.2	E	Intergranular
20-2, 50-59	SB	6	26	H	0.3	0.7	0.2	—	0.4	1.6	—	3.2				0.3	E	Intergranular
20-2, 62-65	SB	6	26	H	4.0	0.5	0.3	—	1.0	1.2	—	7.0				—	E	Vitrophyric-intersertal
22-2, 63-67	PC	7	58	J	—	1.0	—	3.0	1.0	6.0	1.0	12.0			d	0.5	E	Tachylitic
22-2, 77-82	PB	7	58	J	—	1.8	—	2.7	2.0	6.2	0.9	13.6	m		d	0.3	C	Tachylitic-variolitic
25-2, 39-45	ST	8	78	K	—	2.0	—	4.0	1.0	7.0	1.0	15.0			d	2.0	E	Intersertal
27-1, 12-18	ST	8	83	K	—	3.0	—	3.0	1.0	5.0	1.0	13.0			d	1.5	E	Intersertal
30-3, 13-16	PB	9	94	L	1.0	2.0	0.1	1.0	2.5	4.0	1.0	11.6	m		m	2.0	E	Vitrophyric-variolitic
32-1, 1-6	PT	9	104	M	2.0	2.2	—	0.4	1.2	3.8	2.0	11.6	d		m	1.0	C	Vitrophyric-variolitic
32-1, 27-31	PC	9	104	M	1.5	3.2	—	0.4	1.1	2.6	2.1	10.9	d		m	2.4	C	Intersertal with segregation vesicles
32-1, 44-50	PC	9	104	M	1.4	1.1	—	0.4	1.5	5.2	2.3	11.9	d		m	0.7	C	Tachylitic
32-1, 90-94	PB	9	104	M	2.0	1.6	—	tr	1.2	3.9	2.8	12.5	d			1.0	C	Variolitic
Hole 485A																		
11-3, 57-60	PT	1	1	A	—	3.3	—	—	—	—	0.7	4.0				0.2	C	Vitrophyric-variolitic
11-3, 116-121	PC	1	1	A	—	2.5	—	—	—	—	0.2	2.7				—	E	Intersertal
12-1, 10-16	PC?	1	2	B	—	—	—	—	—	—	—	2.7				—	C	Tachylitic-ophimottled
12-1, 76-82	PC?	1	3	C														Intersertal
13-1, 110-117	SC	1	5	E														Intersertal
30-3, 38-41	SC	5	9	I														Ophitic
30-4, 8-13	SC	5	9	I														Ophitic
36-3, 65-69	PB?	7	11	K	0.3	1.2	—	tr	0.8	2.2	3.1	7.6	d			—	C	Tachylitic-vitrophyric
39-1, 26-32	SC	8	12	L														Subophitic

Note: PT = pillow top; PC = pillow center; PB = pillow bottom; ST = sheet flow top; SC = sheet flow center; SB = sheet flow bottom; d = Dominant type of glomerocryst; m = Minor type of glomerocryst.

^a After Flower et al. (this volume).

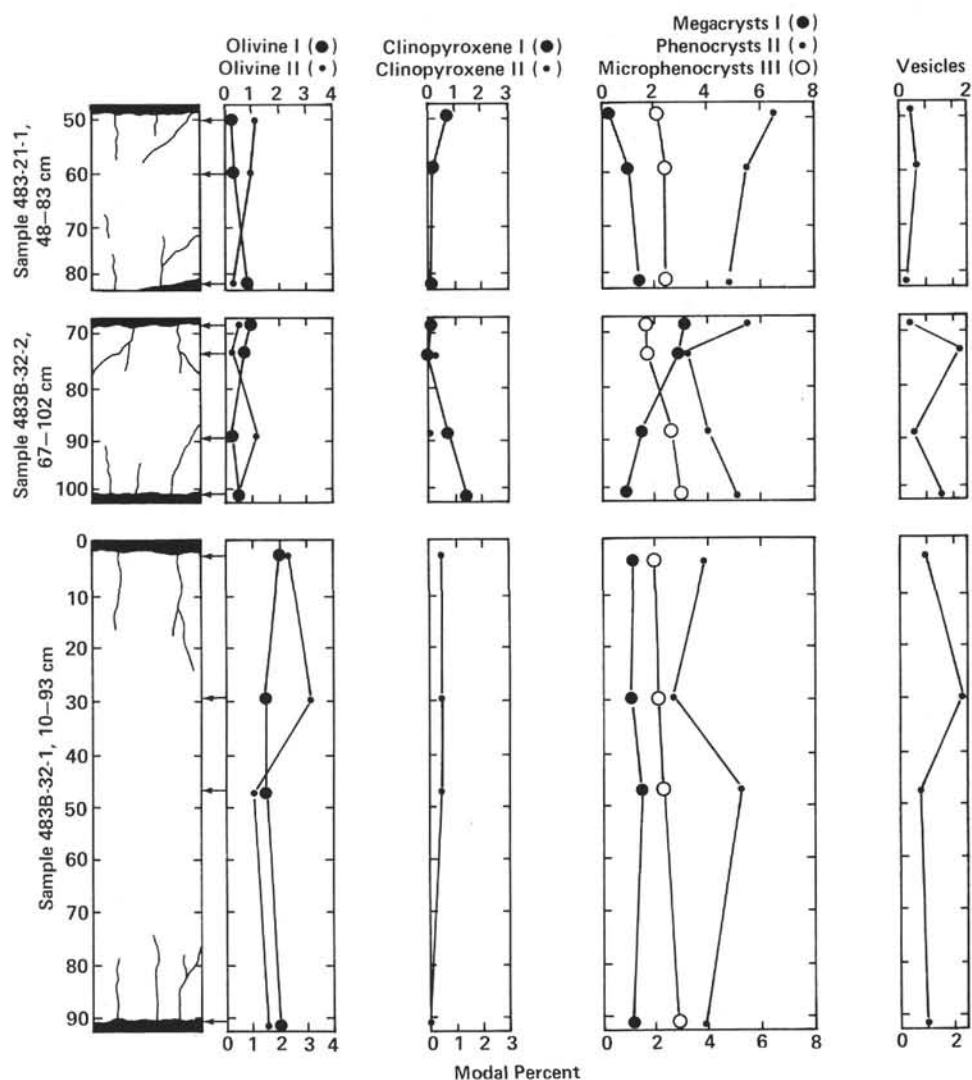


Figure 5. Modal variation of different generations of phenocrysts in three pillow lava units from Holes 483 and 483B.

usually acicular in form, with aspect ratios as high as 15 and areas ranging from 0.01 to 0.5 mm², with a mean of less than 0.1 mm² (Figs. 6 and 7). The plagioclase in this group occurs in varying amounts (generally less than 3%) in the glassy selvages of pillows and flows; therefore, it must have crystallized prior to emplacement, even though its morphology is similar to that of microlites. In general it can be distinguished from groundmass plagioclase in the glassy or tachylitic rinds of pillows and flows, but not in the more slowly cooled interiors of the thicker cooling units.

Plagioclase IV (groundmass microlites): The plagioclase crystals belonging to Group IV resemble the microlites of Group III but show wide variations in texture and shape which depend principally on the cooling rate (Lofgren, 1974; Kirkpatrick, 1979; Natland, 1978; Kuo, 1980).

Clinopyroxene

Clinopyroxene occurs in three forms in the Leg 65 basalts. These consist of large isolated phenocrysts, small phenocrysts, and microphenocrysts and microlites.

Clinopyroxene I (normal phenocrysts): The phenocrysts in this group occur either as single, large (≤ 2 mm), rounded crystals (Plate 4, Fig. 2) or in intergrowths with euhedral to subhedral plagioclase. The crystals are grass green in hand specimen and occur exclusively in the phyric pillow basalts of Holes 483 and 483B, where they constitute less than 1% of the rock.

Clinopyroxene II (phenocrysts and microphenocrysts): The crystals belonging to Group II are euhedral to anhedral and are generally about 0.5 mm in diameter. They occur chiefly in glomerocrysts with plagioclase (Plate 4, Figs. 3 and 4) and constitute less than 2% of the rock.

Clinopyroxene III (microlites): The clinopyroxene crystals belonging to Group III occur in all of the thicker cooling units drilled on the leg.

Olivine

Olivine occurs in three forms in the basalts recovered on Leg 65. These consist of megacrysts and phenocrysts, microphenocrysts, and groundmass crystals.

Olivine I (megacrysts and phenocrysts): The olivine megacrysts observed contain spinel inclusions, are slight-

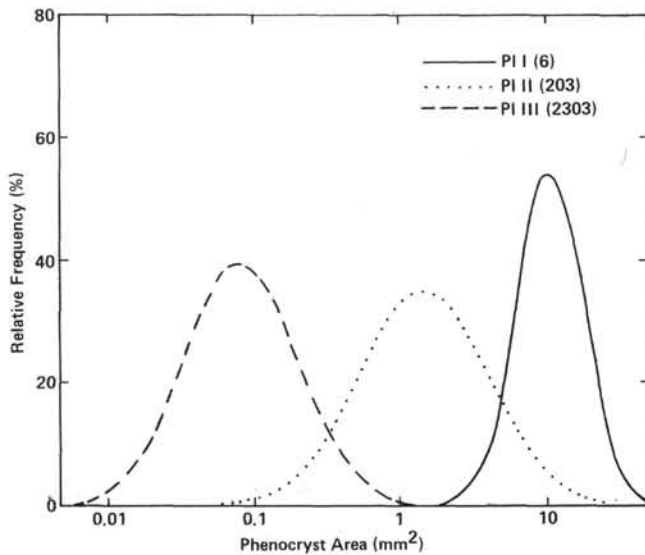


Figure 6. Relative frequency vs. cross-sectional area of phenocrysts belonging to different generations of plagioclase found in Leg 65 basalts. (PI I, megacrysts; PI II, phenocrysts; and PI III, microphe- nocysts. Numbers in parentheses represent numbers of mea- surements.)

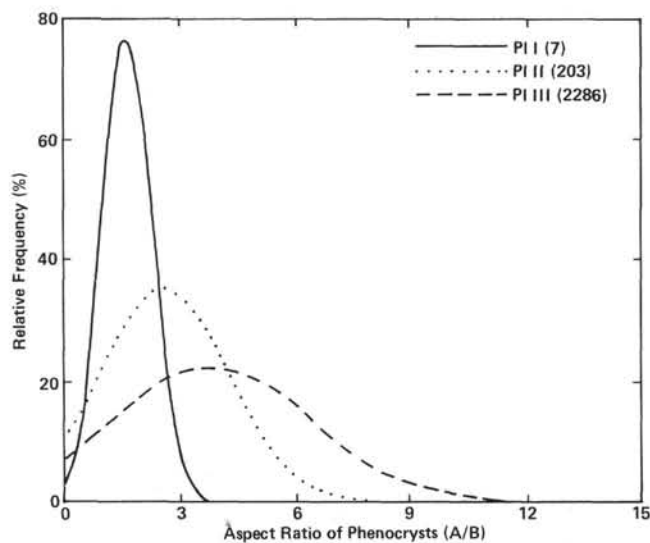


Figure 7. Relative frequency vs. aspect ratio of phenocrysts belonging to different generations of plagioclase found in Leg 65 basalts. (PI I, megacrysts; PI II, phenocrysts; and PI III, microphe- nocysts. The peaked distribution for PI I indicates that the megacrysts generally have low length/width ratios while the flatness of the PI III curve reflects the high length/width ratios of acicular plagioclase. The plagioclase phenocrysts (PI II) show an intermediate distribution of aspect ratios. Numbers in parentheses represent numbers of measurements.)

ly rounded, and occur as rare, single crystals up to 12 mm in length. The more common euhedral phenocrysts may be present in clots with plagioclase and, more rarely, with clinopyroxene phenocrysts.

Olivine II (microphe- nocysts): The crystals belonging to Group II are generally less than 2 mm long, show skeletal growth forms (Plate 3, Fig. 4; Plate 4, Fig. 1)

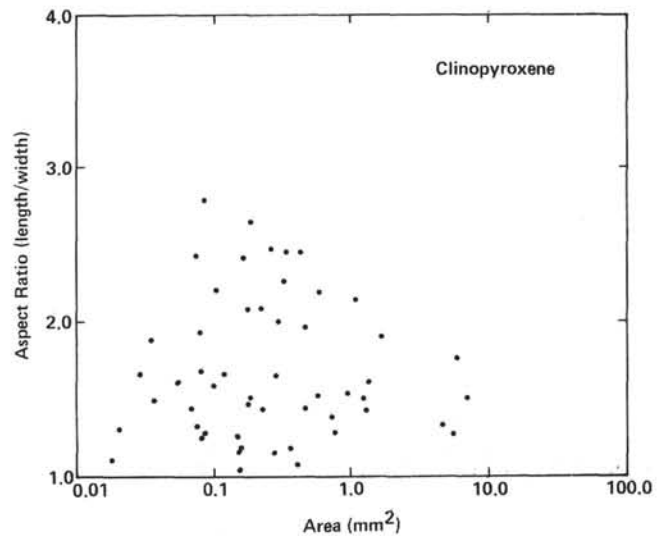


Figure 8. Aspect ratio vs. cross-sectional area of clinopyroxene crystals in Leg 65 basalts. (Note the relative abundance of small crystals with high length/width ratios. The low ratios shown for crystals with small areas result from crystals with long axes inclined to the plane of the thin section.)

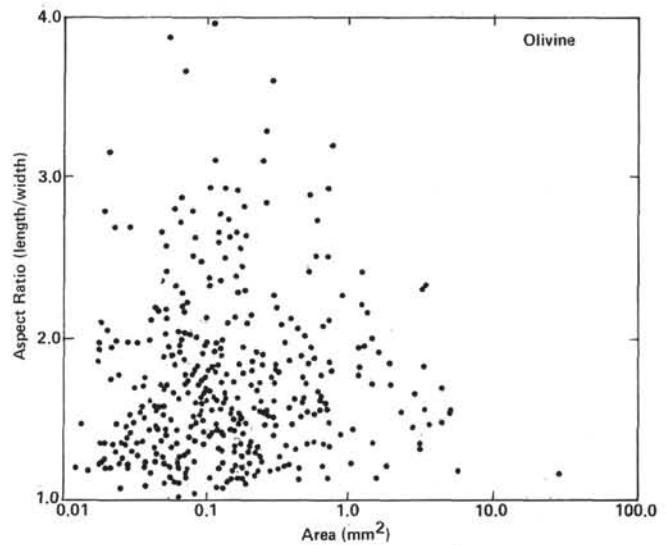


Figure 9. Aspect ratio vs. cross-sectional area of olivine crystals in Leg 65 basalts.

and occur in glomerophytic clots with plagioclase or, more rarely, as single crystals.

Olivine III (groundmass olivine): Groundmass olivine is common in the highly crystallized interiors of massive basalts, but it is generally replaced by alteration products.

Plagioclase/Clinopyroxene Glomerophytic Clots

Three types of plagioclase/clinopyroxene clots with gradations between all types are recognized in the Leg 65 basalts. These include: (1) small clots, generally 1.0 mm in length, of strained anhedral clinopyroxene and acicular plagioclase (Plate 4, Fig. 4); (2) intergrowths of moderately coarse-grained, subhedral to euhedral clino-

pyroxene and plagioclase (Plate 4, Fig. 3), and rare clots of rounded clinopyroxene and plagioclase; and (3) subophitic to ophitic clots of anhedral clinopyroxene and plagioclase ranging up to 5 mm in length. These are distinct from the clinopyroxene/plagioclase clots that form *in situ* in the zone between the chilled margin and the fully crystallized interior of the thicker cooling units.

Petrographic Relationships

A number of conclusions may be drawn from the observations that have been presented. For example, it is clear that plagioclase phenocrysts are much more abundant in the Leg 65 basalts than are olivine and clinopyroxene phenocrysts but that a wide spectrum of assemblages is observed, including plagioclase + olivine, plagioclase + clinopyroxene, plagioclase + olivine + clinopyroxene, and olivine + spinel. It is also evident that each of the major phenocryst phases may appear in several different forms, such as megacrysts, normal phenocrysts, microphenocrysts, and microlites. Finally, it is apparent that the pillow units at Site 483 are distinctly more porphyritic than the massive basalts but that intra-cooling-unit variation in phenocryst volumes and proportions within the pillow basalts are negligible.

The occurrence of different assemblages and amounts of phenocrysts is clear evidence that crystal fractionation is likely to have played a major role in the evolution of these magmas. However, the diversity in textural types within a given rock indicates that single-stage, closed-system fractionation is not a realistic model for their generation. We interpret the phenocryst textures and different types of clots in terms of several different sites and dynamic conditions of crystallization. Of these, the cooling history appears to be the most important controlling factor. Crystals grown at slow cooling rates are larger and more equant (Figs. 7, 8), a physical relationship that is accentuated by the relatively high degree of resorption of these crystals occurring under disequilibrium conditions subsequent to their crystallization. Possible mechanisms for the resorption of early formed crystals include either a decrease in pressure accompanied by contraction of the primary plagioclase field or an influx of hot magma into a more evolved, cooler magma and the selective concentration of plagioclase as a result of flotation (see also Flower et al., this volume). The last generation of microphenocrysts, on the other hand, commonly displays a skeletal habit (Plate 4, Fig. 1), suggesting crystallization under rapid cooling conditions high in the section.

Apart from the high-pressure(?) megacrysts, the majority of phenocrysts are interpreted as having crystallized in the central magma chamber under the ridge. The occurrence of gabbroic clots indicates the disruption and incorporation of slowly cooled parts of the chamber into ascending magma. Although the phenocryst assemblages, amounts, and textures reflect a wide range in the degree of crystallization, the highly porphyritic varieties encountered in several holes in the Atlantic were not found, possibly indicating more rapid replenishment of the magma reservoirs.

The general lack of significant variation in phenocryst abundance within the pillows (Fig. 5) indicates the intrusion of well-mixed, homogeneous magmas. Even where such variation is significant, as in the base of several of the massive sheet flows in Hole 483B, it is interpreted as being the result of post-eruptive crystal settling.

The more porphyritic nature of the pillows as a whole is not unique to Site 483 but has also been observed in several holes in the Atlantic. A systematic relationship is also suggested by the observation that thin sheet flows of a more fractionated, but related chemical composition underlie the pillow lavas (Flower et al., this volume). In such eruptive cycles, the sheet flows possibly represent the upper part of zoned magma chambers. Pillow sequences have also been observed to overlie sheet flows in the Galapagos Rift zone (Ballard, 1979) and a gradation toward more mafic composition is common in the eruptive cycles observed in the Atlantic (Flower and Robinson, 1979, 1981).

GEOCHEMISTRY

SAMPLE SELECTION AND METHODS

After the petrographic studies had been completed, 15 representative basalt samples were chosen for detailed microprobe studies of mineral composition and three additional samples were chosen for glass analysis. About 600 analyses were obtained on these samples at the Max-Planck Institute für Chemie in Mainz using a KEVEX 5100 energy dispersive analytical system attached to an ARL-SEM-Q microprobe. An additional 80 analyses were obtained using an automated CAMEBAX microprobe. Glass analyses were carried out using a defocused beam. Particular attention was paid to compositional variations within single crystals. Representative mineral and glass analyses are given in Tables 3 through 9, and the average mineral and glass compositions are summarized for selected basalt samples in Table 10.

Mineral Chemistry

Olivine

The olivine phenocrysts and microphenocrysts analyzed from Holes 483 and 483B are chemically homogeneous within each sample. The compositions range from Fo_{81.3} for the microphenocrysts examined in Section 483-21-3 to Fo_{86.2} for the phenocrysts in Section 483B-30-3 (Table 3). These olivine crystals are neither in equilibrium (Roedder and Emslie, 1970) with the glass in the groundmass (where present) (Table 10), nor with possible "primary" magma compositions. This indicates that at the time of olivine crystallization, these lavas had already undergone some degree of fractionation.

Clinopyroxene

Most of the clinopyroxenes examined consist of augite (Tables 4, 5). The more primitive phenocryst cores fall in the endiopside field while the groundmass crystals range from endiopside toward ferroaugite and subcalcic augite in composition (Tables 4, 5; Fig. 10). The phenocryst core compositions are notably uniform in their major element chemistry (100 Mg/Mg + Fe²⁺ = 84.86; Ca₄₁Mg₅₁Fe₈); in accordance with their relatively primitive major element chemistry, they contain minor Cr₂O₃ (1.0–1.3%) and relatively little TiO₂ (0.3%).

Table 3. Composition of selected olivine phenocrysts.

Component	Sample (interval in cm)											
	483-21-3, 6-9	483-22-2, 85-88	483B-22-1, 26-32 (core)	483B-22-1, 26-32	483B-30-3, 13-16 (core)	483B-30-3, 13-16 (rim)	483B-30-3, 18-22 (core)	483B-30-3, 18-22 (rim)	483B-32-1, 1-6	485A-11-3, 68-73	485A-11-3, 68-73	485A-11-3, 116-121
Major oxide (wt.%)												
SiO ₂	39.29	39.78	39.24	39.29	40.44	39.42	41.18	40.61	39.60	40.87	39.61	38.64
FeO ^a	17.57	15.73	17.65	17.76	12.87	16.99	12.25	15.45	15.05	12.88	17.53	11.80
MnO	0.22	0.24	0.14	0.21	0.15	—	0.18	0.15	—	0.22	0.28	0.17
MgO	42.41	44.11	42.47	42.06	46.85	43.48	47.34	45.11	44.44	46.56	42.81	48.62
CaO	0.25	0.28	0.19	0.21	0.22	0.14	0.32	0.26	0.17	0.34	0.36	0.32
NiO	n.a.	0.16	n.a.	n.a.	0.29	n.a.	n.a.	n.a.	n.a.	n.a.	n.a.	0.33
Total	99.73	100.30	99.70	99.52	100.82	100.02	101.37	101.64	99.25	100.87	100.59	99.88
Cation proportions ^b												
Si	10.015	10.001	10.007	10.041	9.980	9.980	10.047	10.035	10.013	10.062	10.007	9.637
Fe	3.744	3.308	3.763	3.796	2.657	3.596	2.498	3.193	3.181	2.652	3.704	2.461
Mn	0.047	0.051	0.031	0.045	0.031	—	0.038	0.032	—	0.046	0.060	0.036
Mg	16.112	16.531	16.140	16.020	17.235	16.407	17.214	16.616	16.748	17.089	16.124	18.077
Ca	0.067	0.076	0.052	0.056	0.059	0.038	0.083	0.084	0.045	0.090	0.097	0.086
Ni	n.a.	0.032	n.a.	n.a.	0.057	n.a.	n.a.	n.a.	n.a.	n.a.	n.a.	0.066
Total	29.985	29.990	29.993	29.959	30.020	30.020	29.927	29.960	29.987	29.939	29.992	30.363
Fo (mole%)	81.1	83.3	81.1	80.8	86.6	82.0	87.2	83.8	84.0	86.6	81.3	88.0

^a FeO* represents total iron as FeO.^b Proportions shown on a basis of 40 oxygen atoms.

Plagioclase

The plagioclase megacrysts, phenocrysts, and groundmass crystals studied vary widely in composition from An_{91.7} to An_{36.1} (Tables 6, 7; Fig. 11), the extent of differentiation varying according to the mode of occurrence. The phenocrysts and megacrysts display the highest values, the groundmass crystals display the lowest (An₇₃₋₇₆), and the crystals occurring in glomerocrysts (An₇₅₋₆₁) overlap with both. This overlap results in part from the difficulty of distinguishing microphenocrysts from coarse groundmass crystals.

The megacrysts and larger phenocrysts are characterized by strong optical zoning. To investigate the relationship between chemistry and zoning in these crystals, successive analyses were made from rim to rim and from core to rim across eight crystals at various intervals (40–200 μm) depending on the crystal size. The most calcic phenocryst examined (Sample 485A-39-1, 26–32 cm) shows a uniform core (An₉₁) with a narrow, relatively sodic central zone (An₈₀) and an abrupt decrease in An content at the rims to groundmass values (An₄₄). Other calcic phenocrysts, however, show more systematic decreases in An content toward the rims (e.g., Sample 483B-20-2, 50–59 cm). Minor reversed zoning is also present. The less calcic phenocrysts (An₇₀₋₈₀) are more varied in their chemical zonation, with some being uniform (e.g., Sample 483-21-3, 6–9 cm) and others irregular (Sample 483-22-2, 85–88 cm). Interestingly, nearly all show asymmetric zonation.

Clinopyroxene and Plagioclase Glomerocrysts

The clinopyroxene/plagioclase glomerocrysts examined display a relatively restricted range of feldspar and clinopyroxene compositions (An = 75–61; Mg No. = 85–77). These two parameters show a fairly positive covariant relationship with a correlation coefficient (for

14 samples) of 0.848. This suggests that the glomerocrysts represent coliquidus phases from magmas having different degrees of evolution. However, such a linear relationship cannot be extrapolated to the most calcic plagioclase observed (An₉₂) because it would require the coexisting clinopyroxene to have a magnesium number exceeding 100.

DISCUSSION

The phase chemistry that has been discussed demonstrates that the Leg 65 basalts are typical ocean floor basalts. The relatively low Mg/Mg + Fe values of the mafic minerals and glasses also suggest that the basalts are evolved, although it is difficult to determine the extent of this evolution. Petrographically, a crystallization sequence of plagioclase, plagioclase and clinopyroxene, and finally plagioclase, clinopyroxene, and olivine is recognized in the few samples analyzed by microprobe. This is supported by the phase chemistry: moderately evolved plagioclase (An₇₅₋₆₁) occurs with relatively magnesian clinopyroxene (100 Mg/Mg + Fe = 85–77) in glomerocrysts, and magnesium-rich olivine (Fo₈₆₋₈₁) occurs with evolved plagioclase and clinopyroxene microphenocrysts ranging to that of the groundmass compositions.

The feldspar compositions range from strongly calcic (An₉₂) down to groundmass compositions both between grains and within strongly zoned crystals. These observations are in conflict with experimental studies of primitive ocean floor basalts that show that plagioclase more calcic than An₈₀ does not exist as a liquidus phase (Green et al., 1979). The same authors, however, have suggested the existence of primary magmas with high Al₂O₃ contents, very low Na₂O/CaO ratios, and low TiO₂ and K₂O contents, which have segregated from Na-poor, Ti-poor depleted peridotites at very shallow depths leaving a harzburgite residue. Such magmas would precipitate

Table 4. Composition of selected clinopyroxene phenocrysts, Holes 483, 483B, and 485A.

Component	Sample (interval in cm)										
	483-21-3, 6-9	483-21-3, 6-9	483B-20-2, 16-21 (rim)	483B-20-2, 37-42 (core)	483B-20-2, 37-42	483B-20-2, 37-42	483B-20-2, 50-59 (core)	483B-20-2, 50-59 (rim)	483B-20-2, 50-59	483B-20-2, 50-59 (core)	483B-20-2, 50-59 (rim)
Major oxide (wt.%)											
SiO ₂	53.93	51.66	53.69	53.57	53.57	50.02	52.01	50.96	52.96	53.07	49.65
TiO ₂	0.32	0.99	0.21	0.23	0.44	1.15	0.42	0.93	0.37	0.42	1.30
Al ₂ O ₃	1.46	3.77	2.34	2.19	1.28	2.81	3.63	3.93	2.55	3.03	3.89
FeO* ^a	7.74	7.22	4.83	4.77	9.56	11.90	5.21	8.39	6.08	6.03	13.09
MnO	0.13				0.20	0.14				17.50	0.17
MgO	20.03	17.18	18.04	18.13	20.54	16.14	17.32	16.23	17.91	20.32	14.11
CaO	16.32	19.46	21.14	20.58	14.34	16.10	19.99	19.10	19.64		17.55
Na ₂ O		0.14		0.17			0.14				0.30
Cr ₂ O ₃	0.25	0.40	0.73	0.74	0.11		1.30		0.57	0.65	
Total	100.18	100.81	100.98	100.38	100.02	98.26	100.01	99.53	100.09	101.03	100.05
Cation proportions ^b											
Si	19.594	18.833	19.373	19.426	19.560	18.981	18.991	18.882	19.318	19.203	18.696
Al	0.627	1.621	0.994	0.936	0.552	1.256	1.560	1.715	1.098	1.292	1.726
Σ	20.221	20.454	20.367	20.362	20.112	20.237	20.551	20.597	20.416	20.495	20.422
Ti	0.088	0.272	0.058	0.062	0.120	0.329	0.116	0.260	0.102	0.115	0.367
Fe	2.352	2.201	1.456	1.445	2.920	3.775	1.591	2.598	1.854	1.826	4.123
Mn	0.039				0.061	0.096					0.053
Mg	10.845	2.334	9.704	9.797	11.177	9.131	9.424	8.963	9.739	9.440	7.919
Ca	6.352	7.601	8.175	7.996	5.609	6.545	7.821	7.582	7.676	7.880	7.082
Na		0.099		0.121			0.097				0.217
Cr	0.072	0.115	0.209	0.213	0.031		0.375		0.163	0.187	
Σ	19.747	19.622	19.601	19.635	19.917	19.825	19.189	19.403	19.534	19.447	19.760
Total	39.968	40.076	39.968	39.997	40.029	40.062	39.98	40.000	39.950	39.942	40.182
Mg No.	82.2	80.9	86.9	87.1	79.3	70.7	85.6	77.5	84.0	83.8	65.8
Normative composition											
NAC	0.00	0.98	0.00	1.21	0.00	0.00	0.97	0.00	0.00	0.00	0.00
Jd	0.00	0.00	0.00	0.00	0.00	0.00	0.00	0.00	0.00	0.00	2.13
CCR	0.72	0.16	2.02	0.92	0.31	0.00	2.79	0.00	1.64	1.88	0.00
CTi	0.88	2.70	0.58	0.62	1.20	3.27	1.16	2.60	1.03	1.16	3.60
CATs	1.90	5.27	3.40	3.60	1.40	2.97	5.26	5.97	3.67	4.40	3.81
Wo	30.11	33.65	38.02	37.43	26.51	29.40	34.60	33.62	35.41	35.91	31.07
En	54.39	46.32	48.68	48.99	55.72	45.37	47.24	44.81	48.94	47.47	38.88
Fs	11.99	10.92	7.30	7.23	14.86	18.99	7.98	12.99	9.32	9.18	20.51

Note: NAC = NaCr (Si₂O₆); Jd = NaAl (Si₂O₆); CCR = CaCr (AlSiO₆); CTi = Tp = CaTi (Al₂O₆); CATs = CaAl (AlSiO₆).

^a FeO* represents total iron as FeO.

^b Proportions shown on a basis of 60 oxygen atoms.

the calcic plagioclase and magnesian clinopyroxene observed in ocean floor basalts. Such an origin requires magma mixing at oceanic spreading ridges. Rhodes and Dungan (1979) discuss this latter question in some detail based on residual glass compositions and compositional variations in olivine and plagioclase phenocrysts. They suggest that mixing and crystal contamination between upwelling primary magmas and evolved magmas in a steady-state magma chamber beneath the ridge give rise to a "buffered" ocean floor basalt magma. However, since none of the residual or included glass compositions match the composition suggested by Green et al. (1979) a primary magma origin is considered unlikely for the calcic phenocrysts considered in this study. It is also interesting to note that while Rhodes and Dungan (1979) found plagioclase values as high as An₈₅ in liquidus runs on Leg 45 basalts, they did not find plagioclase as calcic as the natural phenocryst compositions.

The disparities observed between experimental work and natural rocks demonstrate the existence of a fundamental problem with respect to the petrogenesis of ocean floor basalt. Clearly an understanding of the

genesis of highly calcic plagioclase phenocrysts is vital to determining the origin and evolution of ocean floor basalts. The Leg 65 results demonstrate the existence of a continuum of feldspar compositions to values as high as An₉₂ within samples from one area. The presence of this compositional continuum is inconsistent with the existence of a uniform steady-state magma chamber since it demands wide variations in the conditions of crystallization. Since experimental studies on primitive basalts have failed to reproduce the range of phenocryst compositions seen in submarine basalts and studies of natural glass inclusions (Rhodes and Dungan, 1979) fail to support the existence of magmas other than those observed on the ocean floor, it is clear that the experimental results must be used with caution until the methodology of experimental petrology has been improved.

ACKNOWLEDGMENTS

We are grateful to the Deutsche Forschungsgemeinschaft for providing financial support for this research (Schm 250/24 and 26). We also wish to thank G. Pritchard for providing a number of mineral analyses; the Max Planck Institut für Kosmochemie (Mainz) and K. Abraham (Ruhr-Universität Bochum) for allowing us to use their

Table 4. (Continued).

Sample (interval in cm)											
483B-22-1, 28-32 (core)	483B-22-1, 26-36	483B-22-2, 63-67	483B-22-2, 63-67	483B-22-2, 77-82	483B-22-2, 77-82	483B-25-2, 39-45	483B-25-2, 39-45 (core)	483B-25-2, 39-45	483B-27-1, 12-18 (core)	483B-30-3, 13-16	483B-32-1, 1-6 (core)
52.77	52.19	53.67	52.00	51.69	53.21	50.38	52.89	52.86	52.06	53.44	54.18
0.42	0.95	0.25	0.51	0.84	0.47	1.44	0.47	0.31	0.55	0.42	0.25
2.84	3.78	1.53	2.53	3.35	1.87	2.90	3.29	1.79	3.33	1.79	1.85
6.15	7.17	6.33	8.55	8.07	7.08	11.95	6.27	8.91	6.15	6.83	6.23
				0.25	0.20	0.24					
17.57	16.85	18.73	17.20	16.37	18.03	14.34	17.62	18.74	17.13	19.74	19.71
20.16	19.47	18.34	18.27	19.32	18.47	18.85	20.08	16.67	20.08	17.05	18.12
				0.28	0.22				0.24		
0.61	0.28	0.33					0.70	0.11	0.67	0.60	0.77
100.52	100.70	99.78	99.06	100.17	99.55	100.11	101.31	99.39	100.22	99.86	101.10
19.207	19.002	19.615	19.305	19.038	19.538	18.912	19.101	19.491	19.038	19.459	19.477
1.218	1.620	0.659	1.109	1.454	0.809	1.282	1.399	0.777	1.436	0.766	0.785
20.425	20.622	20.274	20.414	20.492	20.347	20.194	20.500	20.268	20.474	20.225	20.262
0.115	0.261	0.068	0.143	0.233	0.130	0.408	0.128	0.086	0.153	0.115	0.067
1.872	2.184	2.118	2.655	2.486	2.174	3.752	1.893	2.747	1.882	2.079	1.873
				0.078	0.062	0.077					
9.532	9.194	10.205	9.518	8.989	9.870	8.026	9.483	10.297	9.337	10.712	10.558
7.863	7.583	7.181	7.268	7.624	7.266	7.583	7.768	6.587	7.870	6.653	6.977
				0.200	0.157				0.170		
0.176	0.082	0.095					0.200	0.032	0.193	0.173	0.219
19.557	19.264	19.667	19.583	19.610	19.569	19.845	19.471	19.750	19.605	19.732	19.693
39.982	39.886	39.941	39.997	40.102	40.006	40.039	39.971	40.018	40.079	39.957	39.955
83.6	80.7	82.8	78.2	78.3	81.9	68.1	83.4	78.9	83.2	83.7	84.9
0.00	0.00	0.00	0.00	0.00	0.00	0.00	0.00	0.00	1.69	0.00	0.00
0.00	0.00	0.00	0.00	1.98	1.57	0.00	0.00	0.00	0.00	0.00	0.00
1.78	0.83	0.96	0.00	0.00	0.00	0.00	2.01	0.32	0.23	1.74	2.20
1.15	2.64	0.68	1.43	2.31	1.30	4.06	1.28	0.86	1.52	1.15	0.67
4.07	5.14	2.15	4.12	3.90	1.96	2.32	4.73	2.86	5.49	1.82	2.17
35.89	34.10	34.22	33.58	34.63	34.68	34.57	34.94	30.86	35.42	31.05	32.52
47.78	46.25	51.33	47.60	44.49	49.32	39.97	47.55	51.39	46.32	53.79	53.03
9.38	11.05	10.65	13.28	12.69	11.17	19.07	9.49	13.71	9.34	10.44	9.41

microprobe facilities; A. Fischer and K. Bauszus for drafting and photography; and V. Helmke for typing the manuscript.
facilities; A. Fischer and K. Bauszus for drafting and photography; and V. Helmke for typing the manuscript.

REFERENCES

- Ballard, R. D., 1979. The Galapagos Rift at 86°W: 3. Sheet flows, collapse pits, and lava lakes of the rift valley. *J. Geophys. Res.*, 84:5407-5422.
- Flower, M. F. J., and Robinson, P. T., 1979. Evolution of the FAMOUS ocean ridge segment: Evidence from submarine and deep sea drilling investigations. In Talwani, M., Harrison, C. G., and Hayes, D. E. (Eds.), *Deep Drilling Results in the Atlantic Ocean: Ocean Crust*. Sec. Maurice Ewing Series: Washington (Am. Geophys. Union), 314-330.
- _____, 1981. Basement drilling in the western Atlantic Ocean 2. A synthesis of construction processes at the Cretaceous ridge axis. *J. Geophys. Res.*, 86:6299-6309.
- Green, D. H., Hibberson, W. O., and Jaques, A. L., 1979. Petrogenesis of Mid-ocean Ridge Basalts. In McElhinny, M. W. (Ed.), *The Earth: Its Origin, Structure and Evolution*: London (Academic Press) pp. 265-299.
- Kirkpatrick, R. J., 1979. Processes of crystallization in pillow basalts, Hole 396B, DSDP Leg 46. In Dmitriev, L., Hejrtzler, J., et al., *In-
it. Repts. DSDP*, 46: Washington (U.S. Govt. Printing Office), 271-282.
- Kuo, L.-C., 1980. Morphology and zoning patterns of plagioclase in phryic basalts from DSDP Legs 45 and 46, Mid-Atlantic Ridge [M.A. dissert.]. University of Illinois.
- Lofgren, G., 1974. An experimental study of plagioclase crystal morphology: Isothermal crystallization. *Am. J. Sci.*, 274:243-273.
- Natland, J. H., 1978. Crystal morphologies in basalts from DSDP Site 395, 23°N, 46°W, Mid-Atlantic Ridge. In Melson, W. G., Rabinowitz, P. D., et al., *Init. Repts. DSDP*, 45: Washington (U.S. Govt. Printing Office), 423-445.
- Rhodes, J. M., and Dungan, M. A., 1979. The evolution of ocean-ridge basaltic magma. *Deep Drilling Results in the Atlantic Ocean: Ocean Crust*. Sec. Maurice Ewing Series: Washington (Am. Geophys. Union), pp. 262-272.
- Robinson, P. T., Flower, M. F. J., Swanson, D. A., et al., 1980. Lithology and eruptive stratigraphy of Cretaceous oceanic crust, western Atlantic Ocean. In Donnelly, T., Francheteau, J., Bryan, W., Robinson, P., Flower, M., Salisbury, M., et al., *Init. Repts. DSDP*, 51, 52, 53, Pt. 2: Washington (U.S. Govt. Printing Office), 1535-1556.
- Roedder, P. L., and Emslie, R. F., 1970. Olivine-liquid equilibrium. *Contrib. Mineral. Petrol.*, 29:275-289.
- Schmincke, H.-U., Rautenschlein, M., Robinson, P. T., and Mehgan, J., in press. Accretionary processes inferred from the Troodos Extrusive Series, Cyprus. *Earth Planet. Sci. Lett.*

Table 4. (Continued).

Component	Sample (interval in cm)										
	483B-32-1, 1-6 (rim)	483B-32-1, 1-6 (core)	483B-32-1, 1-6 (rim)	485A-12-1, 76-82	485A-13-1, 110-117	485A-30-3, 38-41	485A-30-4, 8-13	485A-30-4, 8-13	485A-30-4, 8-13	485A-39-1, 26-32	485A-39-1, 26-32
Major oxide (wt.%)											
SiO ₂	51.67	51.71	51.51	51.02	52.02	52.80	53.03	53.86	51.78	50.75	52.47
TiO ₂	0.59	0.64	0.93	1.16	0.73	0.63	0.55	0.84	0.71	1.08	0.65
Al ₂ O ₃	3.83	3.86	4.55	3.73	2.79	1.59	1.91	1.72	1.69	3.77	2.01
FeO ^a	5.37	5.78	6.13	7.46	7.52	8.68	6.34	10.89	9.72	8.03	11.07
MnO				0.20	0.22	0.27	0.19	0.33	0.16		0.27
MgO	16.65	16.93	17.24	15.90	17.10	17.50	17.21	16.01	15.81	15.59	17.63
CaO	20.89	20.26	20.03	19.93	18.76	17.79	20.28	18.04	18.75	20.38	16.46
Na ₂ O	0.28		0.29	0.21	0.23	0.21	0.22	0.25			
Cr ₂ O ₃	1.39	0.87	1.20							0.33	
Total	100.68	100.05	101.89	99.64	99.37	99.46	99.73	101.94	98.62	99.94	100.49
Cation proportions ^b											
Si	18.832	18.917	18.567	18.891	19.224	19.531	19.351	19.603	19.474	18.799	19.337
Al	1.645	1.665	1.935	1.628	1.215	0.693	0.837	0.738	0.749	1.647	0.871
Σ	20.477	20.582	20.502	20.519	20.439	20.229	20.188	20.341	20.223	20.446	20.208
Ti	0.162	0.176	0.253	0.323	0.203	0.175	0.154	0.230	0.201	0.302	0.181
Fe	1.638	1.717	1.849	2.310	2.324	2.685	1.927	3.315	3.057	2.488	3.392
Mn				0.063	0.069	0.085	0.060	0.102	0.051		0.084
Mg	9.048	9.231	9.264	8.777	9.421	9.651	9.542	8.687	8.864	8.606	9.681
Ca	8.158	7.942	7.734	7.960	7.428	7.051	8.081	7.035	7.555	8.088	6.501
Na	0.197		0.202	0.151	0.165	0.151	0.159	0.176			
Cr	0.401	0.251	0.342							0.097	
Σ	19.604	19.367	19.644	19.584	19.610	19.798	19.923	19.545	19.728	19.581	19.839
Total	40.081	39.949	40.146	40.103	40.049	40.022	40.111	39.886	39.951	40.027	40.047
Mg No.	84.7	83.9	83.4	79.2	80.2	78.2	83.2	72.4	74.4	77.6	74.1
Normative composition											
NAC	1.95	0.00	1.99	0.00	0.00	0.00	0.00	0.00	0.00	0.00	0.00
Jd	0.00	0.00	0.00	1.50	1.64	1.51	1.57	1.78	0.00	0.00	0.00
CCR	2.02	2.52	1.38	0.00	0.00	0.00	0.00	0.00	0.00	0.97	0.00
CTi	1.61	1.77	2.49	3.21	2.02	1.75	1.52	2.33	2.02	3.01	1.80
CATs	5.54	5.34	6.35	4.12	3.20	0.96	1.83	0.52	1.74	4.72	2.53
Wo	35.88	35.10	33.01	35.84	34.35	33.82	38.20	34.16	36.08	35.98	30.19
En	44.88	46.39	45.66	43.56	46.88	48.15	47.08	43.94	44.54	42.91	48.18
Fs	8.12	8.88	9.11	11.78	11.91	13.82	9.80	17.28	15.62	12.41	17.30

Table 5. Composition of selected clinopyroxene groundmass crystals.

Component	Sample (interval in cm)												
	483B-20-2, 16-21	483B-20-2, 16-21	483B-20-2, 50-59	483B-20-2, 50-59	483B-20-2, 50-59	483B-20-2, 50-59	483B-22-2, 63-67	483B-22-2, 63-67	483B-27-1, 12-18	483B-27-1, 12-18	485A-39-1, 26-32	485A-39-1, 26-32	485A-39-1, 26-32
Major Oxide (wt.%)													
SiO ₂	50.56	50.88	50.10	52.62	50.58	48.82	49.45	50.58	50.32	50.29	50.79	53.21	51.48
TiO ₂	1.15	1.23	1.15	0.68	1.26	2.18	1.43	1.18	1.06	1.44	0.88	1.46	1.02
Al ₂ O ₃	2.02	2.52	4.37	3.24	3.05	5.67	4.77	3.55	2.10	3.99	2.81	1.28	1.89
FeO ^a	15.57	13.38	8.37	6.29	14.49	11.46	8.84	10.36	15.01	10.20	9.14	11.35	15.07
MnO	0.25	0.21			0.22	0.13	0.12	0.27	0.35			0.21	0.34
MgO	12.74	15.64	16.89	17.67	14.33	19.98	15.61	17.77	14.30	15.09	16.23	18.08	15.64
CaO	17.73	16.02	17.78	19.74	16.76	17.33	19.07	15.42	16.28	18.76	18.38	15.91	15.26
Na ₂ O			0.15	0.17			0.29		0.27	0.22			0.17
Cr ₂ O ₃			0.38	0.51			0.11	0.10		0.21	0.35		
Total	100.0	99.88	99.18	100.93	100.69	100.58	99.68	99.23	99.69	100.20	98.60	100.50	100.87
Cation Proportions ^b													
Si	19.246	19.093	18.616	19.075	18.960	18.133	18.420	18.823	19.131	18.697	19.067	19.582	19.239
Al	0.906	1.113	1.916	1.383	1.346	2.482	2.094	1.557	0.941	1.749	1.244	0.555	0.831
Σ	20.152	20.206	20.532	20.458	20.306	20.615	20.514	20.380	20.072	20.446	20.311	20.137	20.070
Ti	0.328	0.346	0.320	0.186	0.355	0.610	0.400	0.330	0.303	0.402	0.250	0.128	0.287
Fe	4.957	4.200	2.601	1.908	4.541	3.558	2.753	3.223	4.773	3.170	2.869	3.494	4.710
Mn	0.080	0.066			0.071	0.042	0.039	0.085	0.114			0.065	0.108
Mg	7.227	8.745	9.354	9.546	8.007	8.295	8.666	9.856	8.103	8.361	9.083	9.916	8.713
Ca	7.230	6.442	7.079	7.668	6.731	6.896	7.611	6.149	6.631	7.471	7.393	6.273	6.111
Na			0.105	0.121			0.207		0.196	0.162			0.120
Cr			0.112	0.146			0.031	0.031		0.062	0.104		
Σ	19.821	19.798	19.570	19.576	19.706	19.401	19.707	19.673	20.120	19.630	19.698	19.875	20.049
Total	39.973	40.004	40.102	40.034	40.012	40.016	40.221	40.053	40.192	40.076	40.009	40.012	40.119
Mg No.	59.3	67.6	78.2	83.3	63.8	70.0	75.9	74.4	62.9	72.5	76.0	73.9	64.9
Normative Composition													
NAC	0.00	0.00	1.04	1.21	0.00	0.00	0.30	0.00	0.00	0.62	0.00	0.00	0.00
JD	0.00	0.00	0.00	0.00	0.00	0.00	1.72	0.00	1.92	0.99	0.00	0.00	1.19
CCR	0.00	0.00	0.07	0.25	0.00	0.00	0.00	0.31	0.00	0.00	1.04	0.00	0.00
CTi	3.29	3.46	3.17	1.85	3.55	6.09	3.91	3.28	2.97	3.99	2.50	1.28	2.84
CATs	1.25	2.10	6.28	4.91	3.18	6.30	5.47	4.31	0.68	4.19	3.20	1.49	0.68
Wo	33.98	29.41	30.28	34.70	30.26	28.23	32.54	26.63	30.70	32.98	33.56	29.94	28.44
En	36.23	43.70	46.29	47.57	39.99	41.41	42.39	49.02	39.75	41.49	45.37	49.52	43.05
Fs	25.25	21.32	12.87	9.51	23.03	17.97	13.66	16.45	23.97	15.73	14.33	17.77	23.81

Note: NAC = NaCr (Si₂O₆); Jd = NaAl (Si₂O₆); CCR = CaCr (AlSiO₆); CTi = Tp = CaTi (Al₂O₆); CATs = CaAl (AlSiO₆).

^a FeO* represents total iron as FeO.

^b Proportions shown on a basis of 60 oxygen atoms.

Table 6. Composition of selected plagioclase phenocrysts, Holes 483, 483B, and 485A.

Component	Sample (interval in cm)												
	483-21-3, 6-9 (rim)	483-21-3, 6-9 (core)	483-21-3, 6-9 (core)	483B-8-1, 24-27	483B-8-1, 24-27	483B-13-1, 60-64	483B-13-1, 60-64	483B-20-2, 16-21 (rim)	483B-20-2, 16-21	483B-20-2, 16-21 (core)	483B-20-2, 37-42 (core)	483B-20-2, 37-42 (core)	483B-20-2, 37-42 (rim)
Major oxides (wt.%)													
SiO ₂	48.15	52.44	49.69	47.83	47.52	48.03	49.35	53.62	48.13	49.75	50.41	52.40	58.73
TiO ₂				0.04		0.04	0.04						
Al ₂ O ₃	33.51	30.01	32.50	33.32	32.99	32.63	31.96	28.57	34.09	31.71	32.51	30.38	25.76
FeO ^a	0.52	0.52	0.40	0.38	0.39	0.52	0.52	0.88	0.29	0.37	0.45	0.44	0.66
MnO						0.02	0.02						
MgO	0.18	0.25	0.24	0.18	0.17	0.17	0.11	0.27	0.17	0.13	0.26	0.30	0.16
CaO	16.55	13.22	15.82	17.17	17.11	16.49	15.60	11.67	17.34	14.75	15.58	13.56	8.06
Na ₂ O	1.92	3.94	2.51	1.74	1.74	2.04	2.56	4.90	1.68	3.02	2.65	3.95	7.22
K ₂ O		0.05	0.07		0.01	0.01	0.01	0.08			0.06	0.06	0.12
SrO						0.04	0.06						
Total	100.82	100.42	101.24	100.66	99.96	99.99	100.21	100.00	101.69	99.73	101.92	101.08	100.71
Cation proportions ^b													
Si	8.763	9.494	8.985	8.731	8.741	8.824	9.018	9.738	8.690	9.108	9.044	9.435	10.471
Al	2.188	6.404	6.926	7.169	7.152	7.065	6.883	6.116	7.255	6.842	6.875	6.448	5.412
Σ	15.951	15.898	15.911	15.900	15.893	15.889	15.901	15.845	15.945	15.950	15.919	15.883	15.883
Ti				0.005		0.006							
Fe	0.079	0.078	0.061	0.058	0.060	0.080	0.079	0.134	0.043	0.057	0.067	0.066	0.098
Mn						0.003	0.003						
Mg	0.049	0.067	0.066	0.049	0.047	0.047	0.030	0.073	0.046	0.035	0.069	0.080	0.043
Ca	3.226	2.564	3.065	3.358	3.372	3.246	3.054	2.271	3.354	2.894	2.994	2.616	1.540
Na	0.678	1.382	0.881	0.616	0.621	0.727	0.907	1.726	0.587	1.071	0.923	1.378	2.494
K		0.012	0.017		0.002	0.002	0.002	0.019			0.014	0.130	0.027
Sr						0.004	0.006						
Σ	4.031	4.103	4.089	4.086	4.102	4.115	4.086	4.223	4.031	4.057	4.067	4.153	4.201
Total	19.982	20.001	20.000	19.986	19.995	20.004	19.987	20.077	19.976	20.007	19.986	20.036	20.084
An(mole%)	82.6	64.8	77.3	84.5	84.4	81.7	77.1	56.5	85.1	73.0	76.2	65.3	37.9

^a FeO^{*} represents total iron as FeO.

^b Proportions shown on a basis of 32 oxygen atoms.

Table 6. (Continued).

Component	Sample (interval in cm)												
	483B-25-2, 39-45	483B-25-2, 39-45 (core)	483B-25-2, 39-45	483B-27-1, 12-18	483B-27-1, 12-18	483B-27-1, 12-18	483B-30-3, 13-16 (core)	483B-30-3, 13-16	483B-30-3, 13-16 (core)	483B-32-1, 1-6	483B-32-1, 1-6 (core)	483B-32-1, 1-6	483B-32-1, 1-6 (rim)
Major oxides (wt.%)													
SiO ₂	55.49	48.77	52.06	50.15	48.22	52.20	46.33	51.61	48.62	51.99	47.26	48.63	53.67
TiO ₂													
Al ₂ O ₃	27.46	31.54	30.21	31.19	32.53	30.35	33.89	30.48	32.64	30.17	33.29	32.34	28.86
FeO ^a	0.87	0.32	0.49	0.41	0.31	0.54	0.33	0.59	0.21	0.56	0.32	0.31	0.83
MnO													
MgO	0.14	0.26	0.23	0.28	0.13	0.27	0.35	0.29	0.21	0.34	0.22	0.22	0.45
CaO	10.26	15.14	13.37	14.60	15.91	13.46	17.54	13.84	15.99	13.59	17.16	15.77	12.49
Na ₂ O	5.70	2.67	3.88	3.04	2.09	3.84	1.25	3.66	2.36	3.71	1.53	2.25	4.55
K ₂ O	0.09		0.06	0.06		0.06				0.10			0.18
SrO													
Total	100.04	98.70	100.30	99.72	99.19	100.63	99.69	100.45	100.03	100.45	99.79	99.53	101.02
Cation proportions ^b													
Si	10.029	9.034	9.444	9.180	8.895	9.442	8.551	9.363	8.898	9.426	8.699	8.938	9.669
Al	5.849	6.885	6.458	6.729	7.071	6.449	7.373	6.517	7.039	6.446	7.221	7.005	6.128
Σ	15.878	15.919	15.902	15.90	15.966	15.891	15.924	15.880	15.937	15.872	15.920	15.943	15.797
Ti													
Fe	0.135	0.050	0.074	0.063	0.048	0.082	0.051	0.089	0.032	0.085	0.049	0.048	0.125
Mn													
Mg	0.037	0.071	0.062	0.076	0.037	0.072	0.097	0.077	0.059	0.093	0.062	0.061	0.120
Ca	1.987	3.004	2.599	2.863	3.144	2.608	3.469	2.689	3.135	2.639	3.385	3.105	2.411
Na	1.996	0.959	1.365	1.078	0.748	1.346	0.448	1.287	0.838	1.302	0.547	0.802	1.589
K	0.022		0.013	0.014		0.015				0.023			0.041
Sr													
Σ	4.177	4.084	4.114	4.093	3.977	4.123	4.063	4.142	4.064	4.142	4.043	4.017	4.285
Total	20.055	20.003	20.016	20.002	19.943	20.014	19.987	20.022	20.001	20.014	19.963	19.960	20.082
An(mole%)	49.6	75.8	65.4	72.4	80.8	65.7	88.6	67.6	78.9	66.6	86.1	79.5	59.7

Table 6. (Continued).

Sample (interval in cm)														
483B-20-2, 50-59 (rim)	483B-20-2, 50-59	483B-20-2, 50-59	483B-20-2, 50-59	483B-20-2, 50-59	483B-20-2, 50-59	483B-20-2, 50-59 (core)	483B-20-2, 50-59 (rim)	483B-22-1, 26-32 (rim)	483B-22-1, 26-32	483B-22-1, 26-32	483B-22-2, 63-67 (rim)	483B-22-2, 63-67 (core)	483B-22-2, 63-67 (core)	483B-22-2, 77-82
53.39	51.38	46.58	49.68	50.29	47.52	49.10	58.70	53.76	50.95	48.47	54.46	49.65	51.37	52.14
29.41	30.42	33.59	32.42	31.57	33.04	32.40	25.33	28.49	30.06	31.92	29.10	31.85	30.54	29.57
0.71	0.49	0.33	0.39	0.40	0.35	0.45	0.70	0.72	0.55	0.35	0.86	0.34	0.51	0.70
0.25	0.30			0.27	0.24	0.20		0.32	0.29	0.18	0.30	0.25	0.23	0.20
12.56	13.83	17.09	15.41	14.96	16.62	15.94	7.63	11.98	13.50	15.43	12.25	15.26	13.85	13.64
4.40	3.48	1.15	2.63	2.91	1.82	2.27	7.26	4.65	3.43	2.34	4.79	2.60	3.65	3.57
				0.06	0.06		0.12	0.05	0.06	0.05	0.08	0.06	0.10	0.01
														0.06
100.72	99.90	98.73	100.53	100.45	99.65	100.36	99.74	99.98	98.84	98.74	101.85	100.02	100.23	99.99
9.628	9.364	8.654	9.029	9.143	8.753	8.956	10.549	9.756	9.383	8.977	9.717	9.070	9.344	9.497
6.521	6.533	7.354	6.945	6.766	7.174	6.965	5.366	6.093	6.525	6.969	6.119	6.857	6.547	6.348
16.149	15.897	16.008	15.974	15.909	15.927	15.921	15.915	15.849	15.908	15.946	15.836	15.927	15.891	15.845
0.107	0.075	0.052	0.059	0.061	0.053	0.068	0.105	0.109	0.085	0.054	0.128	0.051	0.077	0.107
0.066	0.082			0.072	0.067	0.055		0.087	0.079	0.050	0.081	0.069	0.061	0.054
2.426	2.700	3.401	3.001	2.914	3.280	3.114	1.470	2.330	2.663	3.062	2.341	2.987	2.699	2.662
1.540	1.231	0.413	0.927	1.026	0.649	0.805	2.528	1.636	1.224	0.839	1.656	0.919	1.286	1.261
				0.013	0.015		0.028	0.012	0.014	0.013	0.019	0.014	0.023	0.002
														0.006
3.68	4.088	3.867	3.987	4.085	4.064	4.043	4.131	4.173	4.065	4.018	4.225	4.041	4.143	4.006
20.017	19.985	19.875	19.961	19.994	19.991	19.964	20.046	20.022	19.973	19.964	20.061	19.968	20.034	19.951
61.2	68.7	89.2	76.4	73.7	83.2	79.5	36.5	58.6	68.3	78.2	58.3	76.2	67.3	67.8

Table 6. (Continued).

Sample (interval in cm)													
485A-11-3, 68-73	485A-12-1, 76-82	485A-13-1, 110-117	485A-13-1, 110-117	485A-30-3, 38-41	485A-30-4, 8-13	485A-30-4, 8-13	485A-30-4, 8-13	485A-39-1, 26-32	485A-39-1, 26-32	485A-39-1, 26-32 (core)	485A-39-1, 26-32 (rim)	485A-39-1, 26-32	485A-39-1, 26-32
50.16	51.82	51.87	56.15	52.06	53.34	51.22	50.11	50.89	57.06	45.38	53.71	48.69	53.36
0.08	0.08	0.06	0.15	0.06	0.11	0.06							
31.08	29.55	30.07	27.12	29.08	29.01	30.16	29.83	30.85	26.56	34.66	28.97	32.71	29.16
0.59	0.67	0.63	1.10	0.72	0.76	0.60	0.55	0.45	0.62	0.26	0.80	0.37	0.67
	0.02	0.02	0.02		0.03	0.02							
0.20	0.25	0.18	0.11	0.09	0.22	0.17		0.28	0.11	0.18	0.19	0.24	0.22
15.09	13.87	14.24	11.06	13.90	12.79	14.14	14.46	14.19	9.28	18.27	12.12	16.17	12.34
3.04	3.69	3.46	5.36	3.85	4.32	3.57	2.74	3.34	6.44	0.99	4.69	2.14	4.63
	0.01		0.01	0.01	0.02	0.02							0.05
0.04	0.06	0.07	0.06		0.07	0.06							
100.28	100.02	100.60	101.14	99.77	100.67	100.02	97.69	100.0	100.07	99.74	100.49	100.32	100.43
9.156	9.452	9.407	10.057	9.520	9.640	9.351	9.346	9.276	10.261	8.391	9.704	8.890	9.652
6.686	6.353	6.427	5.725	6.268	6.179	6.490	6.558	6.628	5.629	7.553	6.169	7.037	6.217
15.842	15.805	15.834	15.782	15.788	15.819	15.841	15.904	15.904	15.890	15.944	15.873	15.927	15.869
0.011	0.011	0.008	0.020	0.008	0.015	0.008							
0.090	0.102	0.096	0.165	0.110	0.115	0.092	0.086	0.069	0.094	0.040	0.120	0.057	0.101
	0.003	0.003	0.003		0.005	0.003							
0.054	0.068	0.049	0.029	0.025	0.059	0.046		0.075	0.029	0.050	0.050	0.066	0.059
2.951	2.711	2.767	2.122	2.723	2.477	2.766	2.890	2.772	1.787	3.619	2.347	3.163	2.391
1.076	1.305	1.217	1.861	1.365	1.514	1.264	0.991	1.181	2.247	0.355	1.644	0.757	1.626
	0.002		0.002	0.002	0.005	0.005							0.012
0.004	0.006	0.007	0.006		0.007	0.006							
4.186	4.208	4.147	4.208	4.233	4.197	4.190	3.967	4.096	4.157	4.065	4.161	4.043	4.189
20.028	20.013	19.981	19.990	20.021	20.016	20.031	19.871	20.000	20.047	20.009	20.034	19.970	20.058
73.3	67.5	69.5	53.2	66.6	62.0	68.6	74.5	70.1	44.3	91.1	58.8	80.7	59.3

Table 7. Composition of selected plagioclase groundmass crystals.

Component	Sample (interval in cm)							
	483B-20-2, 16-21	483B-20-2, 16-21	483B-20-2, 37-42	483B-20-2, 50-59	483B-20-2, 50-59	483B-20-2, 50-59	483B-20-2, 50-59	483B-27-1, 12-18
Major Oxides (wt. %)								
SiO ₂	53.84	56.29	52.77	56.71	52.72	54.19	57.24	52.39
Al ₂ O ₃	29.03	27.07	29.59	27.47	29.38	28.19	27.04	29.61
FeO* ^a	0.78	0.77	0.81	1.05	1.10	0.83	0.79	0.59
MgO	0.22	0.27	0.27	0.05	0.35	0.17	0.08	0.26
CaO	11.86	9.79	12.73	9.90	12.63	12.15	9.63	13.08
Na ₂ O	4.67	8.84	4.32	5.95	4.18	4.47	6.17	4.10
K ₂ O			0.07	0.07			0.09	
Total	100.40	99.76	100.56	101.20	100.34	100.73	101.04	100.04
Cation Proportions ^b								
Si	9.721	10.163	9.550	10.117	9.565	9.754	10.209	9.525
Al	6.179	5.761	6.313	5.775	6.281	6.133	5.683	6.346
Σ	15.900	15.924	15.863	15.892	15.846	15.887	15.892	15.871
Fe	0.117	0.116	0.123	0.156	0.166	0.126	0.118	0.090
Mg	0.060		0.072	0.022	0.094	0.046	0.022	0.071
Ca	2.295	1.893	2.469	1.891	2.455	2.342	1.840	2.548
Na	1.636	2.044	1.515	2.057	1.469	1.559	2.133	1.446
K			0.016	0.012			0.021	
Σ	4.107	4.054	4.196	4.138	4.183	4.072	4.134	4.154
Total	20.007	19.978	20.059	20.030	20.029	19.959	20.026	20.025
An mole%	58.4	48.1	61.7	47.8	62.6	60.0	46.1	63.8

^a FeO* represents total iron as FeO.^b Proportions shown on a basis of 32 oxygen atoms.

Table 8. Composition of selected Fe/Ti-oxides.

Component	Sample (interval in cm)			
	483-22-2, 89-83	483-22-2, 89-83	483-22-2, 89-83	485A-30-4, 8-13
Major oxides (wt. %)				
SiO ₂	0.52			0.55
TiO ₂	22.93	23.94	21.77	21.15
Al ₂ O ₃	5.08	5.16	6.67	1.99
FeO* ^a	68.34	67.48	70.47	71.28
FeO	(51.13)	(52.57)	(51.87)	(49.74)
Fe ₂ O ₃	(19.13)	(16.57)	(20.67)	(23.93)
MnO	0.73	0.48	0.42	0.82
MgO	0.65	0.48	0.41	0.53
CaO	0.33	0.17	0.11	
V ₂ O ₃	0.20		0.37	
Total	98.78	97.99	100.22	96.32
	(100.7)	(99.37)	(101.92)	(98.71)
Cation proportions ^b				
Si	0.187			0.207
Al	2.157	2.230	2.788	0.881
Ti	6.211	6.601	5.807	5.972
Fe ²⁺	15.403	16.119	15.386	15.621
Fe ³⁺	5.196	4.572	5.517	6.762
Mn	0.223	0.149	0.126	0.261
Mg	0.349	0.262	0.217	0.297
Ca	0.127	0.067	0.042	
V	0.058		0.105	
Total	29.911	30.0	29.988	30.001

Note: Recalculated values shown in parentheses.

^a FeO* represents total iron as FeO.^b Proportions shown on a basis of 40 oxygen atoms.

Table 9. Selected glass compositions.

Major Oxides (wt.%)	Sample (interval in cm)						
	483-21-3, 6-9 ^a	483-21-3, 6-9	483-21-3, 6-9	483B-22-1, 26-32	483B-22-2, 77-82	483B-30-3, 13-16	483B-32-1, 1-6
SiO ₂	50.51	50.10	51.69	50.47	51.95	50.24	50.79
TiO ₂	2.04	2.00	2.11	1.94	1.90	1.86	1.73
Al ₂ O ₃	14.35	13.91	14.07	14.00	13.38	13.98	14.35
FeO ^b	11.51	11.40	12.18	11.47	11.43	11.37	10.48
MnO	—	0.17	—	0.13	0.23	—	—
MgO	4.39	7.04	6.90	7.11	6.45	7.15	7.62
CaO	12.60	11.22	11.19	11.37	10.86	11.39	11.96
Na ₂ O	2.58	2.85	0.67	2.91	2.72	2.63	2.85
K ₂ O	0.12	0.08	0.08	0.09	0.07	0.08	0.12
P ₂ O ₅	0.14	0.20	0.14	0.17	—	—	0.11
SO ₃	0.45	0.55	0.53	0.48	—	0.29	0.47
Total	98.70	99.53	99.57	100.16	98.99	99.00	100.48

^a Glass inclusion in olivine.^b FeO^{*} represents total iron as FeO.

Table 10. Average mineral and glass compositions for selected basalts from Holes 483 and 483B.

Sample (interval in cm)	Phenocrysts						Groundmass				
	Olivine		Clinopyroxene			Plagioclase		Clinopyroxene		Plagioclase	Glass
	Crystal Type	Mg No. ^a	Crystal Type	Mg No. ^a	Ca:Mg:Fe	Crystal Type	An (mole%) ^a	Mg No. ^a	Ca:Mg:Fe	An (mole%) ^a	Mg No. ^a
Hole 483											
21-3, 6-9	MP	81.3 (10)	Gl	82.8 (4)	37:52:11	{ P MP	{ 82.6 (12) 65.0 (6)	—	—	—	52.4 (6)
22-2, 85-88	P	83.3 (7)	P	85.6 (6)	41:51:8	{ P MP	{ 83.0 (21) 62.7 (1)	—	—	71.4 (3)	—
26-1, 39-40	—	—	—	—	—	P	75.4 (2)	—	—	—	—
Hole 483B											
20-2, 16-21	—	—	MP	86.9 (4)	42:50:8	P	87.9 (21)	70.6 (3)	40:42:18	64.1 (13)	—
20-2, 37-42	—	—	MP	87.1 (5)	42:51:7	P	76.2 (10)	81.5 (11)	31:56:13	63.2 (7)	—
20-2, 50-59	—	—	GL, MP	85.6 (9)	42:50:8	{ M P	{ 89.2 (6) 81.3 (17)	79.0 (4)	38:47:15	62.1 (5)	—
20-2, 50-59	—	—	M MP	84.1 (7) 84.7 (7)	40:50:10 41:50:9	P	80.3 (22)	74.0 (3)	35:48:17	62.9 (7)	—
22-1, 26-32	P	81.6 (7)	MP, GL	84.0 (14)	40:50:10	P	78.2 (14)	—	—	—	52.5 (7)
22-2, 63-67	—	—	MP, GL	83.1 (15)	40:50:10	P	76.2 (18)	80.7 (3)	31:56:13	64.7 (3)	—
25-2, 39-45	—	—	MP, GL	84.7 (23)	40:50:9	P	75.8 (13)	—	—	69.0 (4)	—
27-1, 12-18	—	—	MP, GL	83.1 (4)	41:49:10	P	80.8 (14)	72.5 (5)	39:44:17	69.3 (3)	—
30-3, 13-16	? P	86.2 (4) 82.9 (6)	MP, GL	84.2 (8)	42:49:9	{ P GL	{ 88.6 (9) 67.6 (1)	—	—	67.6 (3)	53.8 (7)
30-3, 18-22	P	84.5 (2)	—	—	—	P	82.1 (3)	—	—	—	—
32-1, 1-6	MP, P	84.5 (11)	MP, GL	84.9 (12)	36:54:10	P	86.1 (23)	—	—	—	56.9 (10)
39-1, 26-32	—	—	MP, GL	77.7 (6)	42:45:13	{ M GL	{ 91.7 (42) 62.6 (1)	76.0 (6)	38:47:15	70.1 (4)	—

Note: M = megacryst; P = phenocryst; MP = microphenocryst; GL = cpx-pl glomerocryst.

^a Number of analyses in parentheses.

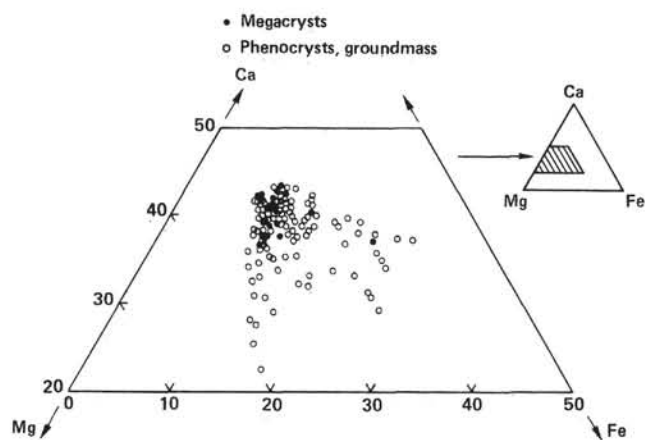


Figure 10. Quadrilateral diagram showing compositions of clinopyroxene megacrysts, phenocrysts, and microphenocrysts in Leg 65 basalts.

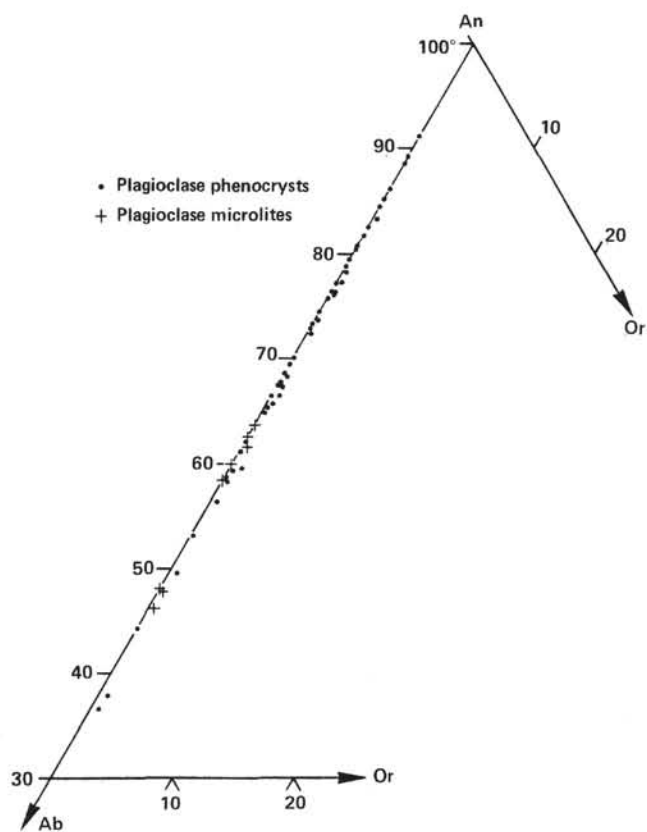


Figure 11. Ternary plot showing selected plagioclase compositions for Leg 65 basalts.

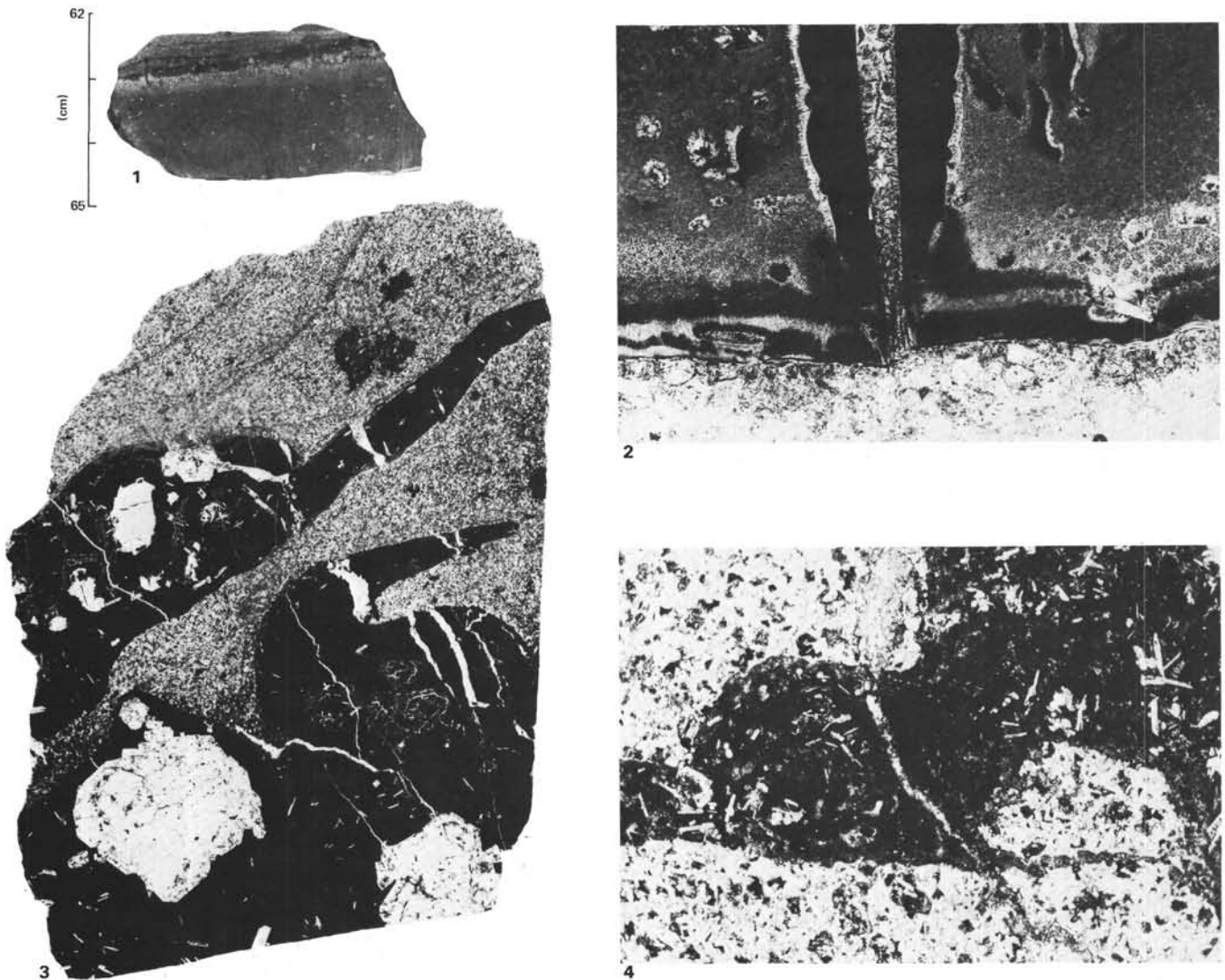


Plate 1. Massive basalts recovered on Leg 65. 1. Sample 483B-20-2, 62-65 cm; thin layer of sandstone adhering to the devitrified base of a massive lava flow (Lithologic Unit 6) (see also Fig. 2.). 2. Sample 483B-20-2, 62-65 cm; basal contact of massive sheet flow(?) (Unit 6) against underlying siltstone (light-colored); glass shows dark alteration against silt and on both sides of straight fracture filled with smectite; glass rinds on massive flows are thinner than on pillows (width of photomicrograph, 5 mm). 3. Sample 485A-38-2, 5-10 cm; cross section through top of deepest massive (intrusive?) basalt drilled in Hole 485A (Lithologic Unit 8) showing devitrified glass stringers in siltstone (width of photograph, 2 mm). 4. Sample 483-16-2, 64-70 cm; fine-grained basalt intruding (self-intruding) medium-grained, massive basalt (Unit 3) (width of photomicrograph, 5 mm).

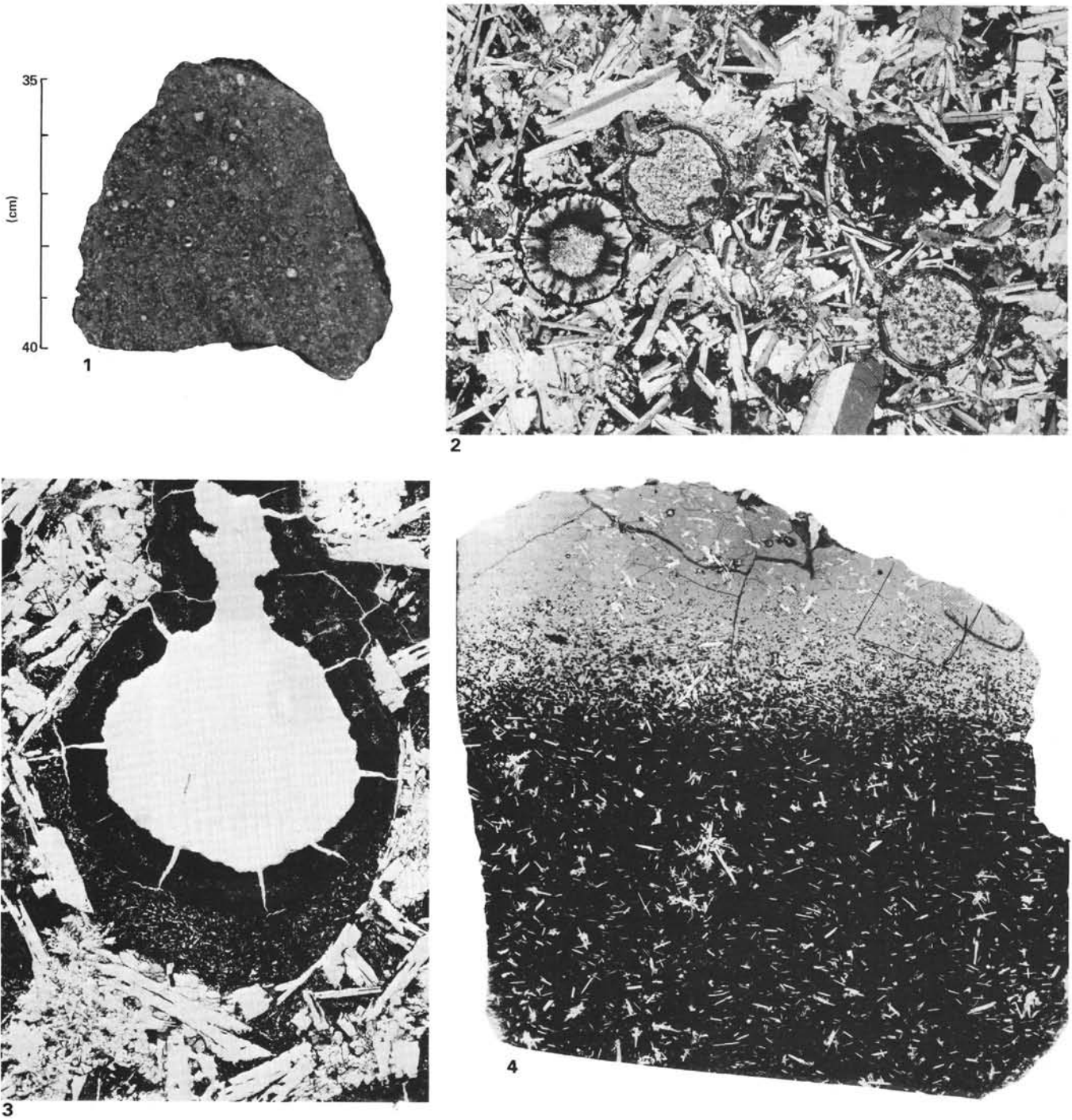


Plate 2. Pillow basalts recovered on Leg 65. 1. Sample 483B-18-2, 35–40 cm; highly vesicular basalt 1.5 meters below top of 3.5-meter-thick massive flow (Lithologic Unit 6) (see also Fig. 3). 2. Sample 483B-26-2, 42–47 cm; massive, vesicular basalt with a coarse-grained, subophitic to interstitial groundmass (Lithologic Unit 8); vesicles to right and center lined with carbonate and filled with smectite; vesicle on left filled with chlorite(?); vesicle to the upper right is a filled segregation vesicle (width of photomicrograph, 5 mm). 3. Sample 483B-18-2, 18–22 cm; partially filled segregation vesicle subsequently lined with smectite(?) showing contraction cracks; note plagioclase laths aligned tangential to vesicle (see Fig. 1) (width of photomicrograph, 5 mm). 4. Sample 482D-11-1, 24–28 cm; cross section through thick, fresh glassy margin of porphyritic pillow lava (50 cm thick) (see also Plate 4, Fig. 1 for photomicrograph of olivine and plagioclase microphenocrysts) (width of photomicrograph, 2 cm).

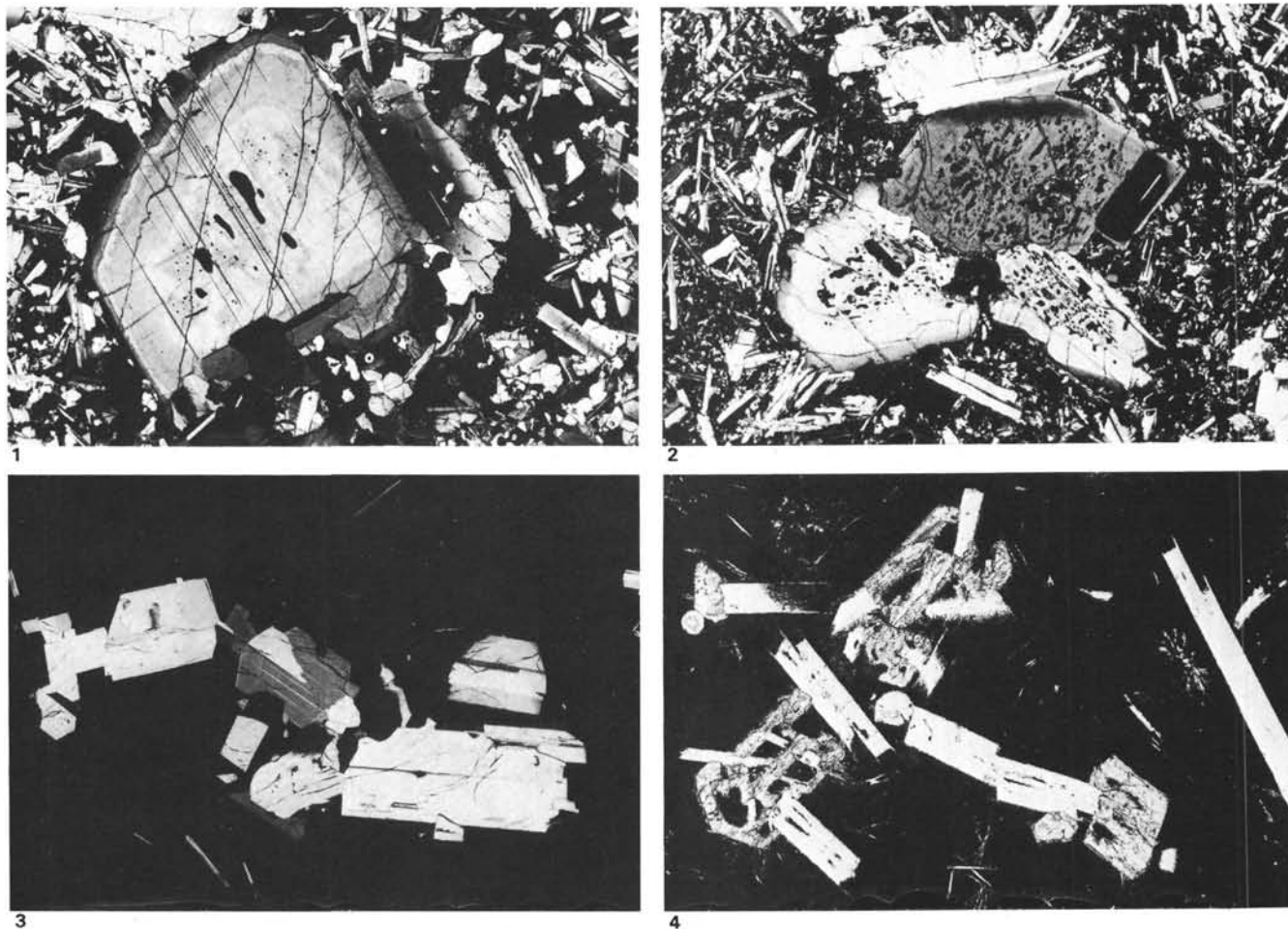


Plate 3. Plagioclase phenocrysts. 1. Sample 483B-7-1, 7-12 cm; plagioclase megacryst in massive flow (Lithologic Unit 3) showing inclusion-rich, partially resorbed core (light gray), an oscillatory zoned mantle, and a dark outer rim separated from the mantle by a sharp compositional break (width of photomicrograph, 5 mm). 2. Sample 483-23-1, 10-16 cm; glomerocryst in pillow basalt (Unit 6) consisting of three partially resorbed plagioclase xenocrysts with numerous glass inclusions and two subhedral plagioclase phenocrysts (width of photomicrograph, 5 mm). 3. Sample 483-21-1, 49-55 cm; euhedral to subhedral clots of regularly zoned plagioclase phenocrysts in tachylitic matrix of pillow basalt (Unit 6) (width of photomicrograph, 5 mm). 4. Sample 485A-36-3, 65-69 cm; clots of skeletal olivine and weakly skeletal plagioclase microphenocrysts in fine-grained pillow basalt(?) (Unit 7) with a tachylitic groundmass containing skeletal plagioclase microlites (width of photomicrograph, 2 mm).

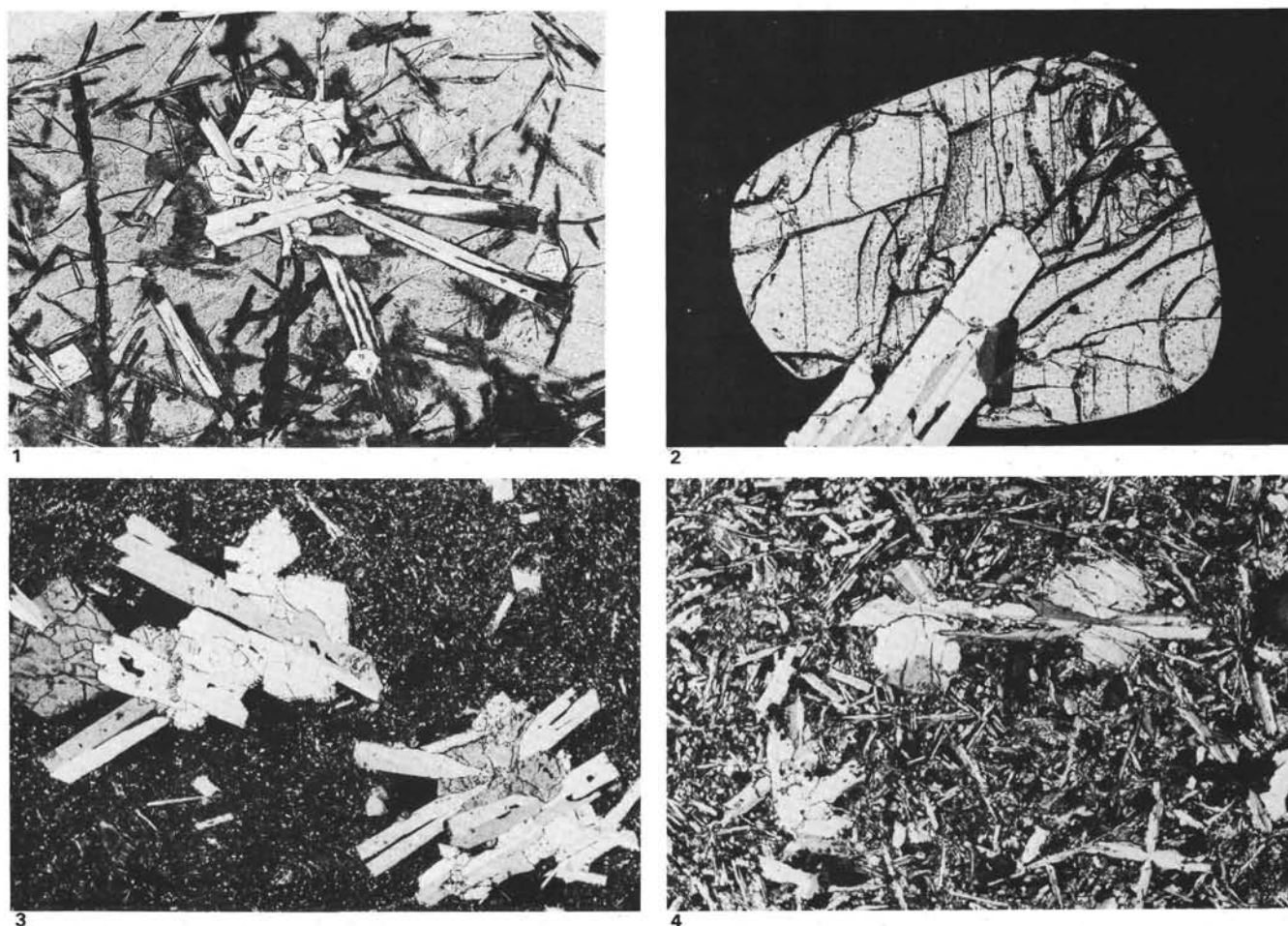


Plate 4. Phenocrysts and clots. 1. Sample 482D-11-1, 24–28 cm; clot of skeletal plagioclase and olivine microphenocrysts in a matrix of fresh sideromelane from the margin of a pillow; microphenocrysts show minor terminal *in situ* growth (width of photomicrograph, 2 mm). 2. Sample 483-22-2, 68–72 cm; partially resorbed clinopyroxene megacryst enclosing euhedral plagioclase phenocrysts in a tachylitic pillow margin (Lithologic Unit 6) (width of photomicrograph, 5 mm). 3. Sample 483-22-2, 77–82 cm; clot of subhedral to euhedral clinopyroxene and plagioclase crystals in a tachylitic pillow margin (Lithologic Unit 6) (width of photomicrograph, 5 mm). 4. Sample 483B-29-1, 55–57 cm; clot of strained anhedral clinopyroxene and plagioclase in an intersertal pillow basalt matrix (Lithologic Unit 9) (width of photomicrograph 5 mm).